Title

Synthesis of Transition Metal Dichalcogenides by Sulfurization of Metal Seeding Layers

Author

Robert, Robert Yem

Publication Date

2023

Peer reviewed|Thesis/dissertation

Synthesis of Transition Metal Dichalcogenides by Sulfurization of Metal Seeding Layers

By

ROBERT COOP

THESIS

Submitted in partial of requirements for the degree of

Master of Science

in

Material Science and Engineering

in the

Offices of Graduate Studies

of the

University of California,

Davis

Approved:

Seung Sae Hong, Chair

Roopali Kukreja

Amir Saeidi

Committee in Charge

2023

Abstract

Transition Metal Dichalcogenides (TMDCs) are strong candidates for a new class of semiconductors due to their tunable bandgaps. Their capacity to stretch and deform makes them suitable for various medical sensors, and TMDCs can be engineered to have thicknesses as low as 1 nm. Despite their potential, producing TMDCs on an industrial scale remains challenging with the current chemical vapor deposition (CVD) methods. The issues stem from the inability to rapidly produce them and the difficulty in maintaining consistency due to multiple sensitive parameters like temperature, pressure, and precursor quantity. A promising alternative is a two-step method, which begins with the sputtering of the transition metal before the CVD process. This approach streamlines the TMDC production process, minimizing variables by automating one of the precursor stages and eliminating the need for manual intervention and catalysts. It's also vital to explore other transition metals since these can alter the TMDCs' properties, particularly their magnetic and superconductive characteristics. In this study, samples were generated using a metal seeding layer method with single coatings of Tungsten and Molybdenum. Dual coatings, including Titanium coated with Molybdenum and Chromium coated with Molybdenum, were tested to inhibit oxidation in the TMDCs. Each sample underwent comprehensive analysis at both the compositional and structural levels including. Raman spectroscopy, X-ray photoelectron spectroscopy (XPS), X-ray diffraction (XRD), and atomic force microscopy (AFM). Whereas Molybdenum disulfide and Tungsten disulfide showed experimental data consistent with the existence of sulfide phases, other materials lack evidence of such sulfurization. The AFM data revealed that the Tungsten disulfide displayed a triangular structure, which is characteristic of this material. While further research on sulfurization of Titanium and Chromium is required, the two-step synthesis approach showed the

potential for broader class of 2D materials including Nickel, Niobium, Vanadium, and more to determine if the metal seeding approach is universally applicable to all TMDCs.

Acknowledgements

I would like to express my thanks to Zach White for helping in the synthesis and data collection of TMDCs samples. I felt like it was an exciting way to get an undergraduate to do some important research and analyzation with atomic force microscopy.

Thank you to professor Sueng Sae Hong for helping guide me through the process of graduation as well as guiding me to learn different types of characterization and synthesis methods during my stay at UC Davis.

In addition, thank you to Hudson Shih, Jieyang Zhou, Huijue Liu, Zoe Wiggins and David Zhou for helping with my research.

Table of Contents

List of Figures and Tables

1 Introduction

Transition Metal Dichalcogenides (TMDCs, also referred to as TMDs) represent a thrilling category of materials, with ongoing evolutionary research. The scientific community is vigorously investigating the diverse properties and possible applications of TMDCs. Their incorporation into practical devices is expected to expand in the forthcoming years as we gain a more profound comprehension of TMDCs substances and enhance manufacturing methodologies. TMDCs materials are known to have a unique structure that is closely related to graphene/graphite [1]. TMDCs are similar due to their hexagonal layers, which are held together by Van der Waals bonds. TMDCs compounds comprise two elements, typically represented by the chemical formula MX_2, where 'M' stands for the transition metal, and 'X' represents the chalcogenide. Both components are interchangeable, with 'M' possibly being Mo, W, Ti, Cr, V, Pt, among others, and 'X' could be S, Se, or Te. Altering either 'M' or 'X' results in variations in properties (including electrical, structural, optical, and magnetic) and affects the synthesis protocols during chemical vapor deposition. It's important to note that the MX_2 structure broadly applies when discussing all TMDC combinations. There are three principal structural variations of TMDCs compounds, known as 1T, 1T', and 2H, and these play a crucial role in determining whether the TMDCs exhibit ferromagnetic or superconductive properties. TMDCs are noted for their utility as dry lubricants and for their adaptable mechanical properties, which are due to the Van der Waals forces present in their structure and their natural propensity for deformation. The aim of utilizing TMDCs materials lies in their application as semiconductors in various industries and technological domains. This is because TMDCs have the unique attribute of exhibiting varied electrical conductivity, electron flow direction, and bandgaps across different layers. TMDCs compounds can be fabricated using methods such as chemical vapor deposition

or atomic layer deposition. Molybdenum disulfide (MoS_2) stands out as the most prominent and extensively studied transition metal dichalcogenide. However, there's potential for enhancing this material by making its production process faster and more consistent. For MoS_2, there's room for greater optimization in its manufacturing. A comprehensive understanding of the various MX_2 combinations is essential to determine their optimal uses and applications in semiconductor technology. TMDCs' unique structure is fundamental to their role in facilitating electron pathways. Their capacity for combining diverse metals and chalcogenides, coupled with the tunability of layers and substrates, enhances their adaptability for various electronic device applications.

1.1 Transition Metal Dichalcogenide Heterostructures

The TMDC materials are characterized by their association with 2H and 1T structures, both of which are hexagonal as depicted in **Figure 1.1**. The image illustrates the structures specific to TMDCs, where the blue atoms represent transition metals, and the orange atoms denote dichalcogenides within the TMDCs. 2H is a rhombus with the space group of the $P6_3/mmc$ space group shown in the red diamond [1], [2]. The 1T structure, like the 2H, also presents as a rhombus, highlighted within the red diamond in the 1T model, and belongs to the P3-m1 space group[2]. 1T' is described as the distorted sub-phase of both 1T and 2H [2]. All materials in the figure below can change phases depending on correct temperature per TMDCs. Note that not all TMDCs are not on this graph because materials with Platinum [3] and Titanium [4] will just be in the 1T state naturally. The Z-Y directions in 1a dictate the single layer which is about three atoms high. When this material has more than one layer, Van der Waals bonds keep the material together. TMDCs structure is heavily dictated by the transition metal's position on

the element table. Molybdenum and Tungsten have a bigger Z number and are associated with

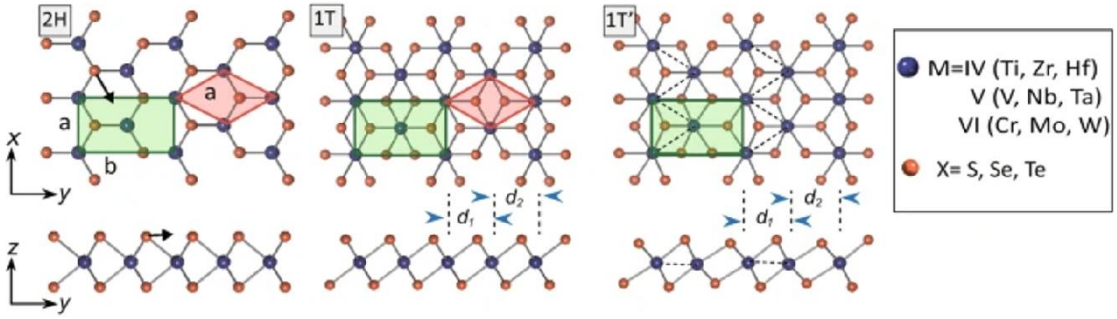

Figure 1.1 *Image indicates the structures for the TMDCs. Blue atoms are the transition metals. Orange are the dichalcogenides in the TMDCs.*

the 2H structure. Titanium, Vanadium, and Chromium have lower Z numbers making them 1T Structures These layer variations are dependent on the techniques that are being used and their recipes that come with them. To successfully make TMDCs there are matching substrates [5] that are needed to make better quality grows such as sapphire [1], silicon oxide [6], gold, graphene [7], GaAs [8], and many other materials that can accommodate the TMDC structure. The higher quality is influenced by the uniformity and spacing of the lattice structure provided by the substrate. One known fact for the MX_2 is that Tungsten Disulfide (WS_2) and MoS_2 are the only TMDCs that form under natural conditions while others MX_2 compounds are not[8]. Some materials such as Chromium and Sulfur have tendencies to go to more favorable structures. For Cr and S, TMDCs like forming a Cr_2S_3 structure which is like 1T structure, but layers relate to Cr bonded to Sulfur and Van Der Waal bonds [9]. 2H, 1T, and 1T' structures underscore the importance of MX_2 TMDCs in semiconductor applications. The conductive and magnetic properties are largely influenced by Van der Waals bonds, lattice parameters, and atomic structures.

1.2 Electrical and Magnetic Properties

Altering M and X elements can result in variations in the electrical properties of TMDCs. One critical aspect under examination is the band gap, which is pivotal for the application of transition metal dichalcogenides in semiconductor functions. The band gap essentially dictates the conductivity properties of TMDCs. $CrSe_2$ naturally assumes a 1T structure, characteristic of metallic materials and exhibits no band gap, whereas MoS_2 adopts a 2H structure, categorizing it as a semiconductor. The number of layers in TMDCs, ranging from a monolayer to multiple layers, also influences their properties. Changing the number of layers can alter the bandgap distance [10]. As the material approaches bulk layer status, the band gap diminishes, thereby increasing the energy required for electron mobility. There's a spectrum of band gap variations depending on the number of layers as well as the combination of materials used. Bulk layers typically exhibit an indirect band gap, while monolayers present a direct band gap[11]. The fewer the layers present, the fewer pathways there are for electron movement. Possessing a monolayer structure result in a larger band gap[12]. Another notable aspect is the relationship between strain and the band gap. Compressive strain exerts a squeezing effect on the structure, while tensile strain pulls it apart. As a result, tensile strain leads to a widening of the bandgap, whereas compressive strain results in a narrowing of the bandgap. The

Table 1.1 *The table presents various phases of distinct TMDCs. An 'F' symbolizes that the material exhibits ferromagnetic properties, while an 'S' signifies superconductivity in the TMDC. 'CDW' denotes the presence of a charge density wave.*

S	Se	Te
Various FeS F	* $FeSe$ F S	
	1T $CrSe_2$ AF	1T $CrTe_2$ F
1T VS_2 F	1T VSe_2 F CDW	1T' VTe_2
2H (1T) TaS_2 F (S)	2H $TaSe_2$ S CDW	1T $TaTe_2$ F
2H MoS_2 S	2H $MoSe_2$ S	2H $MoTe_2$ S
2H NbS_2 S	2H $NbSe_2$ S CDW	1T $NbTe_2$ S
2H WS_2 S	2H WSe_2	1T WTe_2 S
1T TiS_2	1T $TiSe_2$ CDW	1T $TiTe_2$

pursuit of the ferromagnetic properties is particularly driven by their potential applications in spintronic devices[2]. Some TMDCs will have the occurrence of charge density waves or CDWs. With CDWs, there is an unstable distortion in the lattice. This will result in interaction between both phonons and electrons leading to CDWs. CDWs serve as a precursor to superconductors, a crucial aspect in advancing semiconductor technologies. There are different families which can be seen in **Table 1.1**. TMDCs like $CrTe_2$, FeS_2, $TaTe_2$, VTe_2, and VS_2 are a family group that is not superconductive but has ferromagnetic properties that is a sought-out function. Other materials (in green) MoS_2, $MoSe_2$, $MoTe_2$, WS_2, etc. are all non-magnetic and have superconductive capabilities. These features are determined by the 1T and 2H structures and are dependent on transition metal's Z number. Materials like TaS_2 do exhibit the ability to change from one phase to the other, changing their properties. So, at 1T TaS_2 is ferromagnetic and is not superconductive, but can change to a 2H structure via temperature changing its properties. Titanium Dichalcogenides are both non-superconductive and ferromagnetic material. $CrSe_2$ is unique in being an antiferroelectric material. The properties of TMDCs are determined by the structures TMDCs can adopt; the 2H structure tends to exhibit superconductive behavior in semiconductors, while the 1T structure is known for the ferromagnetic quality's desirable in memory storage devices. This results from the alignment of the 1T and 2H structures. The 1T structure, being metallic with a denser atomic arrangement, can generate a magnetic field. In contrast, the 2H structure restricts electron flow more than the 1T does. Additionally, certain TMDCs, depending on their constituent elements, can exhibit charge density waves (CDWs) that may give rise to superconductivity.

1.3 Applications

The primary focus is on the remarkable progress in technology and electronics. One such application is in energy storage development, where TMDCs have the potential to substitute graphite electrodes in batteries. The coveted characteristics of 2H-TMDCs for energy storage include maintaining their structure and possessing significant conductivity compared to traditional Li-ion energy storage[13]. Another electrical capability is creating a supercapacitor [14], [15] to be another form of storage. This capacitor function is contributed by the structure and storage between stacked layers[15]. A feature depending on the number of layers can be used to encourage signals and electricity to travel down specific pathways. An important application that is used for field effect transistors (FETs)[16] because TMDCs can be used as the gate component. These FETs can then be applied to bio, gas, and piezoelectric sensors [15]. Another potential electronic application is spintronics, attributed to magnetic properties. TMDCs are well-suited for spintronics due to their structure, which enables higher energy efficiency in spintronic devices[2]. An upcoming field for these materials is the use for water splitting catalyst action [17]. There are more applications beyond semiconductors such as dry lubricants and aerospace applications. Specifically, MoS_2 is the most discovered TMDC and has a lot of applications for specific properties. MoS_2 can operate as the thin film transistor and characteristic MoS_2 gives is a high on/off current ratio while maintaining great strength making a flexible and desirable transistor [15]. These thin film transistors can then be applied to wear medical devices such as gloves without hindering mobility of the user. The transistor doesn't just pertain to MoS_2 but can be applied to other TMDCs in the same group of family like WS_2. MoS_2 and similar materials have the structure and spacings from the 2H sheets that MoS_2 can effectively be used

as superconductor electrode[15]. Studies have demonstrated that the enhanced energy storage capabilities of MoS2 could make it a promising candidate for use as an anode in lithium-ion batteries because they can operate at lower temperatures[18]. Another set of application MoS_2 can uptake is the use of sensors. These sensors that are being looked at are mainly in the medical field being gas, chemical, glucose, and DNA sensors. For DNA and glucose TMDCs can immobilize large amounts of biomolecules in an area. This is another application for the medical field. MoS_2 sensors can be doped to detect gas. For example, the device can dope with Nitrogen to replace Sulfur to detect NO_2 gas. TMDCs are adaptable to a range of electronic devices and applications, including sensors, transistors, energy storage in batteries, and other electrical components. This versatility renders TMDC materials a desirable choice for incorporation into various devices.

1.4 Chemical Vapor Deposition

Current TMDC's that are made with chemical vapor deposition (CVD) are made with metal oxide powders. There are a lot of CVD methods, but the main one for the purpose of the thesis will be on low pressure chemical vapor deposition (LPCVD) systems. For example, to produce either tungsten or molybdenum disulfide using an oxide like MoO_3 or WO_3 is necessary

to create MoS_2 and similar materials. The most well-known method of CVD can be seen in **Fig. 1.2a** where two precursors in a tube furnace are heated up and deposited onto a substrate. To make TMDCs like MoS_2, two precursors are needed one that can supply the transitional metal, M

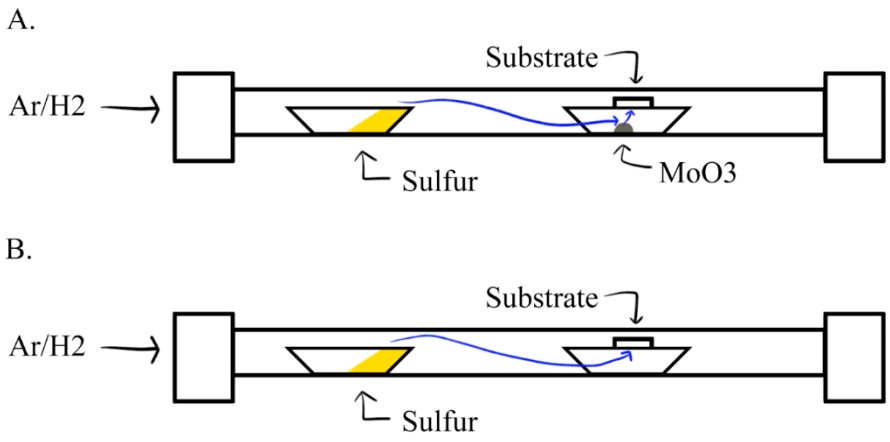

Figure 1.2 *This model shows two methods of CVD for obtaining MoS_2. A) is the normal method involving transition metal oxides. This method uses molybdenum oxide powder and sulfur powders. B) is the seeding method of making the MoS_2.*

and another that can provide X_2 like sulfur. Both the M and X_2 are heated to a temperature to where both precursors will evaporate at. During the whole process Argon (Ar)[19], Argon/hydrogen mix (Ar/H_2), or even Nitrogen(N_2)[6] is flowed through the system to be a means to combine the evaporated sulfur and MoO_3 powder and then will deposit on the bottom of the substrate. Argon is used in the mix since it is a noble gas and does not naturally want to combine with other particles. Hydrogen is used in the system to be combined with the Oxygen molecules to produce water vapor that pump out of the system. 1.2a method can be applied to different TMDCs like tungsten disulfide or Molybdenum selenide. Other TMDCs require slightly more complex precursors to make TMDCs like Titanium (TiS_2). This TiS_2 will require the use of Titanium tetrachloride, $TiCl_4$ with Lithium sulfide Li_2S[12]. Heating the materials will break

apart the precursor and TMDC will form TiS_2 and Lithium Chloride. The problem with CVD comes with the lack of consistency between all CVD machines. TMDCs are all not made equally so the recipes on the CVD machines are always different. Recipes are just setup and procedures of processing the TMDCs. These may include temperature, gas usage, precursor amount and distances between precursors. The primary method of synthesis employs CVD for the effective production of TMDCs. This technique involves the use of Argon mixtures, heat, and precursors to initiate chemical transformation. However, the conventional CVD approach faces significant challenges due to the variability in the parameters of the precursors and furnace conditions, leading to inconsistencies across multiple CVD depositions.

1.5 Metal Seeding Chemical Vapor Deposition

This thesis will revolve around the idea of using a seeding layer. This process will not use MoO_3 or similar powders to create TMDCs but use transition metals as a precursor. The precursor that is being referred to is a layer of metal (Mo, W, Ti, Cr, V, Pt, transitional metal) that is deposited onto the substrate before the CVD process. This deposition is made via physical vapor deposition (PVD) like sputtering, pulse laser deposition, or other PVD processes. Following the PVD process, the metal will be transferred to the CVD system. During the CVD processes when the correct parameters are met the sulfurization of the transitional metal will occur. With this method interesting properties will be formed such as vertical and horizontal layers depending on the thickness of the seeding layer and energy surface[19], [20]. Shown in **figure 1.3** is the possible orientation of the TMDCs structures after processing. For thinner seeding layers there are two possible outcomes seen in figure 1.3b. The horizontal that occurs in low surface energies and the vertical that occurs in higher surface energies[19]. In figure 1.3c,

the thickness is greater than 1 nm, but this allows for uniformed orientations to be achieved. In The thickness of the seeding layer plays a vital role in determining the growth direction of the TMDC layers. With limited growth area, vertical orientation predominates, whereas horizontal growth occurs in conditions with sufficient space. Mixed growth, which is an intermediate between vertical and horizontal orientations, takes place under conditions that fall between these two extremes. In this method this will only produce multiple layers instead of single layers that the other method is seeking[15]. Vertical and horizontal growths can be applied to it can be seen

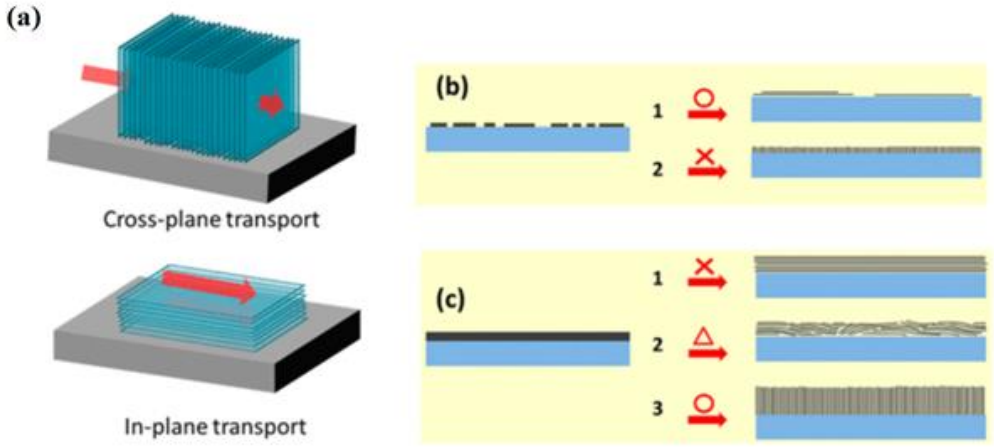

Figure 1.3 *This illustration depicts the two potential alignments the seeding layer can adopt: horizontal or vertical. In 3a, the red arrow illustrates the potential electron flow or current. 3b represents a thin seeding layer, where orientations 1-2 encompass both the vertical and horizontal alignments. In contrast, 3c showcases a more substantial seeding layer, with orientations 1-3 indicating an additional possible alignment.*

in figure 1.3a where the red arrow, representing the flow of electrons, can more likely travel in certain directions. The direction that electrons would be more probable to flow is in the in-plane transport than the cross-plane transport[19]. The reasoning is that for the cross-plane there is a big gap between the atoms with Van der Waals bond that electrons are less favorable to travel.

Horizontal and vertical growth patterns each have distinct electronic applications associated with them. TMDC horizontal layers can be used for electronics and optoelectronics[21] and vertical growths can be used for catalysts for hydrogen fuel cells[17], [21]. Electrons would rather travel in-plane because the electrons use less energy. This vertical and horizontal can then be applied to certain devices that would need a specific electrical path for microelectronics. Seeding CVD also has similar problems with getting the correct thickness and parameters to get the most out of the properties. These horizontal layers can be achieved without using a metal seeding layer by the substrate's position to the crucible it lays on, but non-seeding layer methods are consistent. If the substrate is lying flat on the crucible there will be a horizontal layer created. If the substrate is perpendicular to the flow, there are more vertical growths[22]. Note this using the oxide powder method and not the seeding layer method, but position can have an impact on the angles of interactions. The formation of the structure, either vertical or horizontal, is significantly determined by the thickness of the initial layer deposited through PVD. Studies using the seeding layer method have been used on both MoS_2 and WS_2. Horizontal and vertical configurations can create specific directional pathways along the planes. Nonetheless, a notable drawback of this seeding layer approach is its limited capability in facilitating the growth of monolayers.

1.6 Oxidation of Transition Metal Dichalcogenides

Any oxygen that gets stuck in the CVD system can oxidize the sample which may make characterization of the material harder. Characterization becomes harder because the surface is changed and makes it harder to penetrate or scan from lasers or understand Kikuchi lines. Oxidation effects can also cause discrepancies in the uniform or formations of materials within the sample. Most notable problem with oxidation is some samples made after the CVD method

starts oxidizing in air at room temperature. Steps that can be taken to avoid oxidation are covering layers like Cr and Ti with less oxidizing layers like Mo. The Mo layer can be used as a buffer to separate Ti and open air. Cr, Ti, W, and other transition metals all have different oxidation rates while exposed to air. Notably Tungsten disulfide will oxidize slowly over many weeks, but Titanium disulfide will start oxidizing in minutes. Overall oxidation makes it hard to focus on the wanted structure and morphology of the TMDC sample. Also, water will increase and continue this effect of oxidation over time if the TMDCs are not properly stored or protected. All TMDCs are prone to oxidation, which adversely affects their electrical properties. To mitigate these issues, samples must be shielded with protective coatings, stored in subzero environments, or handled expeditiously to minimize exposure to conditions that catalyze oxidation.

1.7 Project Overview

The fundamental aim of the research is to explore the feasibility of synthesizing additional TMDCs using the metal seeding method. Both Tungsten disulfide and Molybdenum disulfide are examples of materials that have been successfully produced and studied using this seeding layer technique in the past.[13], [19]. The crux of the research is to validate the repeatability and verifiability of this synthesis method through thorough characterization. The overarching significance of this project hinges on determining whether this methodology is scalable for industrial applications. Traditional CVD methods for TMDC are typically more suited to laboratory and research environments. Opting for a two-step process incorporating metal seeding layers is driven by the need for a consistent production method. Utilizing CVD with only a powder precursor may prove problematic because of inconsistent results. In contrast,

Physical Vapor Deposition (PVD) is considered a quicker method since it employs a target source that facilitates consistent deposition. This technique allows for easy sample preparation by simply swapping wafers and substrates in and out of the system, unlike the more traditional CVD methods of weighing metal oxide powders, which can be error-prone and might necessitate an additional catalyst for the process to proceed effectively. Moreover, the traditional CVD method's efficiency is contingent on the sample's placement. Samples synthesized without the seeding layer tend to exhibit smaller areas of growth, whereas the seeding layer method is likely to induce growth areas across the entire sample. Currently, TMDCs do not meet industrial standards and require further refinement for use in semiconductor production. Therefore, the transition metal seeding layer technique stands out as a pivotal method that could offer much-needed consistency in layer thickness and orientation.

2 Synthesis

Synthesis of the material requires two steps. The first step being the physical vapor deposition (PVD) or specifically magnetron sputtering with Argon. PVD is used to deposit the transition metal layer before the sample is subjected to CVD. The metals are either deposited on 500 μm thick Si or Si/SiO wafers that are cut into roughly 10.5x 10.5 mm pieces to be able to fit into the tube furnace. Before PVD process silicon or silicon oxide substrates are subjected to acetone and isopropyl cleaning. In the CVD step all samples are subjected to sulfurization in a vacuumed chamber flowing with Argon or Hydrogen/Argon mix.

2.1 Physical Vapor Deposition of Transition Metals

For deposition of the transition metal (Mo, W, Cr, and Ti) seeding layer, magnetron sputtering. This deposition method is a plasma-based method that requires argon. The sputtering system that was used was the Lesker Labline Sputter in a cleanroom shown in figure 2.1. For sputtering layers, it is necessary to have a charged target that attracts Argon ions[23], [24]. The Argon particles will strike the target creating plasma [23], [24]. This plasma indicates that the metal particles are being ejected and can possibly land onto the desired substrate. The substrate is mounted underneath the target and the substrate is rotated during the deposition process. There are different guns that the targets can be mounted onto. The power used was 100W to slow the deposition rate. Using 300W power results in a greater deposition of layers, as the higher energy level leads to increased attraction of argon atoms to the target. Generally, most metal were deposited with transition metal layers of 40-60 nm or around 3nm in thickness. The chosen thickness proved to be the most effective in producing observable changes and yielded the most

significant results in various characterization analyses. One concerning issue with the PVD system is the buildup metals on the metal protectors that cover the target source. This machine is being used by different groups and some of this build up can possibly end up on the sample during the deposition process.

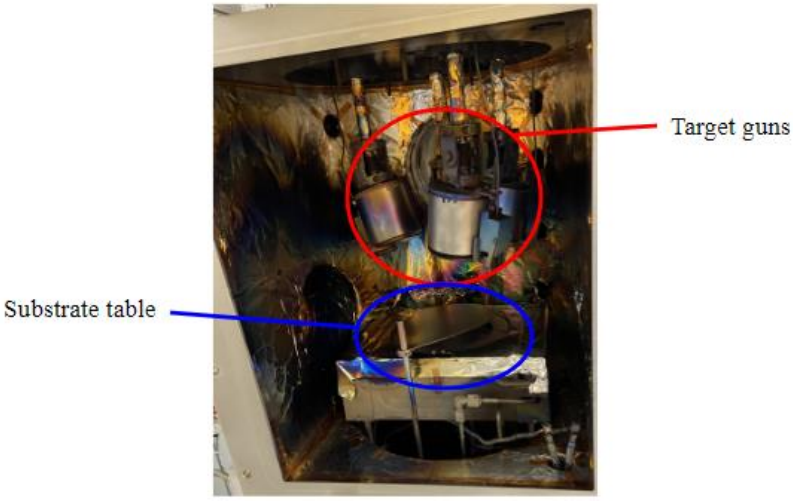

Figure 2.1 *This is the inside of the sputtering machine. In the red is where the target metals are placed, and the blue circle is where the substrate sits. Both shutters are used to start/stop the deposition.*

2.2 Chemical Vapor Deposition of TMDCs

The CVD setup (figure 2.2) is a homemade setup that uses a tube furnace, pump, and filters for the synthesis of the TMDCs. The system is made as a low-pressure CVD. The only thing that is automated is the Lindberg furnace to control the temperature shown in **figure 2.3**. All temperature and time parameters are important since they can alter the growth of the TMDC specimen. The ramp down time (time 3) doesn't ramp down with the input time setpoint because

there is no coolers in the furnace and the only way to quickly cool the system is to open the furnace up without opening the quartz tube. Opening the furnace for cooling down the system can cause different unintended results causing different formation in the TMDC structures or it can stop possible growths within if done too early. The drawback of the CVD system is the

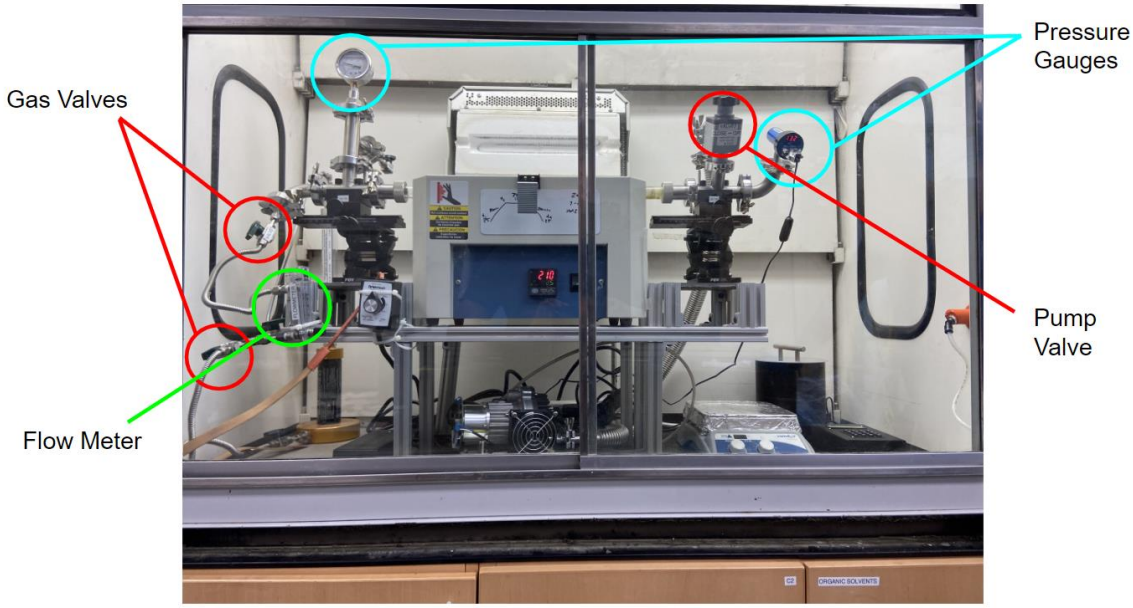

Figure 2.2 *The illustration is Hong lab CVD setup in UC Davis. The system is monitored by both electronic and non-electronic pressure gauges. The dial gauge on the left measures in Torrs and the digital gauge on the right measures in bars. The gas is injected and controlled by the flow meter and the gas valve. Flow meter is in cc/min and gas valves can be turned to Ar or Ar/H_2 gasses to the experimental needs. Lastly on each side of the furnace there is a knob to move the position of the quartz tube in the furnace. The pump valve on the right controls the amount and speed of the gasses leaving the tube.*

absence of a digital mass flow controller, which is essential for regulating the flow rate and pressure of the gases moving through the tube. Instead, the flow must be adjusted by hand with

both the flow meter and pump valve shown in **figure 2.2**. As temperature changes in the CVD chamber so will the flow rate and pressure adding to another layer of possible error during deposition. **Table 2.1** lists the parameters used in the CVD system. The TMDCs made via CVD were Tungsten Disulfide (WS_2), Molybdenum Disulfide (MoS_2), Molybdenum/Titanium Disulfide, and Molybdenum/Chromium Disulfide. Each sample was subjected to the same pressure and flow rate 0.2 Bar and 100 standard cubic centimeters per minute respectively. For the multilayered seeding metals the molybdenum was always deposited last to protect the titanium or the chromium films from oxidation. In the system sulfur powder was used in 0.2 to 0.4 grams to synthesize the TMDCs. The temperatures listed in **Table 2.1** were chosen as the optimal levels to observe a visible change in the samples without risking their integrity. Thickness use was sample that had the best reaction in the CVD system. The 10 nm

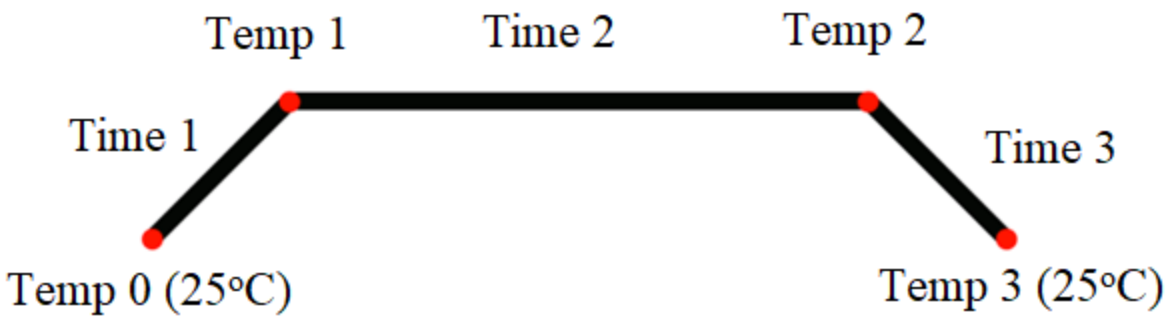

Figure 2.3 *This drawing shows the set points of the furnace. Red dots are temperature set points and the black line represents the timeline of the furnace's processes. Temp 0 is the starting temp and Temp 3 is the end temperature after cooling, both being around room temperature or at 25 C. Time 1 is the ramp up time from start to target temperature of Temp 1. Time 2 is where the temperature is held at the same temperature from Temp 1 to Temp 2. Time 3 is the ramp down from target temperature for the growth back to room temperature.*

layer of Mo used in the double layer structure was implemented to prevent oxidation by shielding the open particles.

Table 2.1 *This shows parameters that were used for depositions in the CVD system. All depositions were run at constant pressure and temperature were held at 15 minutes. Two samples of tungsten were used, one being at 3 nm and the other at 40 nm. Each sample had its respected temperature to enable growth and avoid burning of the surface. Resistant Ratio is the ratio before and after resistance of the synthesis process.*

Seeded Layers	**Temperature**	**Pressure**	**Thickness**	**Time**	**Resistant Ratio**
Molybdenum Disulfide	700°C	0.2 bar	40 nm	15 min	86
Tungsten Disulfide	750°C	0.2 bar	3 nm	15 min	1047
Molybdenum/Titanium Disulfide	800°C	0.2 bar	10 nm Mo 40 nm Ti	15 min	6700
Molybdenum/Chromium Disulfide	800°C	0.2 bar	10 nm Mo 40 nm Cr	15 min	3

Samples below in **Figure 2.4** are the products after the CVD method process. Before CVD synthesis all samples display a silvery color, but after deposition there is a wide variety of optical change in samples that show signs of chemical change. If there was no change in the sample colors this would mean that sulfurization temperature was not reached, and the sample would look the same and may just have burned specks on the surface of the sample. The problem with using optical microscopy is that it can only show changes in colors of the samples and nothing more. Other characterizations are required to be involved in making reasonable conclusions. One method to potentially determine if the samples are TMDCs involves examining their potential. To determine whether the TMDCs experienced a resistance alteration, all samples

were evaluated before and after synthesis using a voltmeter capable of measuring up to 20 KΩ in resistance. In Table 2.1, the resistance ratio reflects the variance encountered during the CVD process. Metals, typically having low to negligible resistance, will display lower values, while oxide and TMDC materials exhibit higher numbers. Monitoring the percentage change is the simplest method to verify if a substance is undergoing a chemical transformation. Notably, both Molybdenum and Molybdenum/Chromium samples demonstrated significant resistance fluctuations. In contrast, the resistance shifts for Tungsten and Molybdenum/Titanium were logged at 100% because the post-CVD process readings were marked as overloaded, indicating that the resistance had exceeded the maximum limit of the voltmeter. The sulfurization of Molybdenum layered over Titanium or Chromium results in different resistance values compared to sulfurized Molybdenum alone. Although Molybdenum typically exhibits consistent resistance values, the introduction of a Chromium or Titanium layer alters these values even before sulfurization.

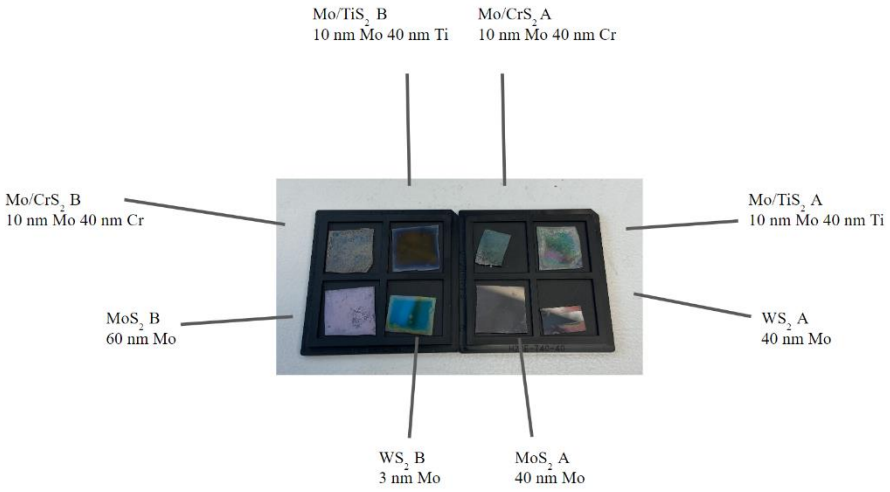

Figure 2.4 *This image shows the samples after CVD procedure. All samples are labeled with the thickness of transition metal used. In description of double layered deposition, the on the left is element the material that is on the surface and exposed to air (ex: Mo deposited on top of Ti).*

3 Sample Characterization Methods

In the thesis, characterization techniques such as Raman spectroscopy, X-ray Diffraction (XRD), X-ray Photoelectron Spectroscopy (XPS), and Atomic Force Microscopy (AFM) were employed. Raman spectroscopy and XPS were utilized to verify the composition of the samples, while AFM and XRD were used to confirm the structure of the TMDCs.

3.1 Raman Spectroscopy

This technique is commonly used to find the fingerprint or composition of the material[25]. This technique has already been used to find the TMDCs and many other materials shown in figure 3.1(A). Raman uses the interaction between light and sample to measure the vibrations to acquire information like infra-red spectroscopy[25], [26]

3.1.1 Background

Raman works when a laser or light are shot at sample surfaces molecules at the sample will be excited by photon and will produce scattering in **figure 3.1**. The light scatterings will be produced either Rayleigh scattering and Raman Scattering. Note that only Raman scattering has relevance in data collecting. There are six forms of vibration modes that a molecule being wagging, twisting, rocking, symmetrical stretch, bending, and asymmetrical bending. Each molecule under Raman scattering there are three times of Raman scattering that can occur. First being elastic scattering or Rayleigh scattering, where the vibrational energy state of the molecule returns to its original position. The other time of scattering is known as inelastic scattering, where the vibrational energy state ends up higher or lower than the original state. The higher

vibration state is Stokes scattering and the lower is anti-stokes scattering. The following equation is used to find the stoke scattering.

$$h(v_o - v_1) = E_1 - E_o \qquad (1)$$

Where h is Planck's constant, E_o is the original energy of the laser, E_1 is the inelastic scattering energy, v_o is the original frequency, and v_1 is the inelastic. If $E_o > E_1$ and $v_o < v_1$ then the system is anti-stoke scattering. If flipped like $E_o < E_1$ and $v_o > v_1$ then the scattering stokes scattering. To determine the fingers prints of the molecule and materials Raman Spectroscopy compares both the incoming photon and the outgoing to photons. Can be found in the change of energy or in the change of wavelength.

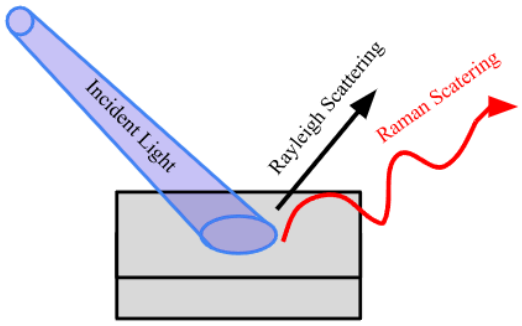

Figure 3.1 *The image is of an incident laser of Raman Spectroscopy hitting the sample. The energy that is being released is the Rayleigh scattering and Raman scattering.*

When measuring TMDCs with Raman spectroscopy there are two distinct peaks that can be seen in **Fig. 3.2A**. The two peaks are the two different vibrations being A_{1g} and E_{2g}, **figure 3.2B**, where the difference is how the atoms of the TMDCs vibrate with one another[20], [27].

Other parameters and factors that need to be accounted for are the amount of TMDC layers. Bulk layers will have different peak positions from monolayers. Bulk layers have the A_{1g} and E_{2g} peaks that are farther away from each other than compared to monolayer that have peaks that are closer to one another[28]. One problem with this machine is that it is destructive to the surface of the samples since lasers are being concentrated into a spot.

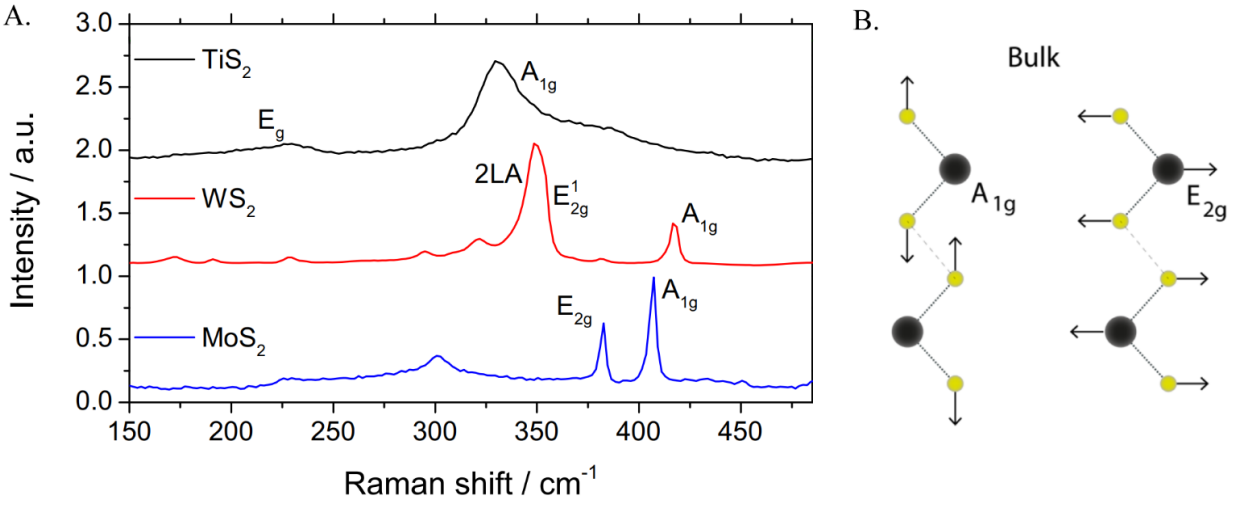

Figure 3.2 *A) shows Raman peaks for TiS_2, WS_2, and MoS_2. These results were using a 532 nm beam with 2,44 eV excitation. B) are the two vibration modes of Bulk TMDCs caused by education from Raman.* [14], [27]

3.2 X-ray Diffraction

The purpose of this characterization is to find the structure of TMDCs materials. Like Raman spectroscopy materials tend to have a specific fingerprint that has already been discovered and be applied to materials.

3.2.1 Background

This device uses x-ray to find planes and structures of crystalline materials[29]. X-ray diffraction or XRD uses the Bragg's Law condition to determine the spacing of the crystalline structure to find the planes. In the **Figure 4.5** below graph both measure intensity and the angle of diffraction. By changing the angle of the X-ray, the planes can be found by the signals that are received. These planes correspond with different structures of each individual material. TMDCs have the same planes associated with them. The diagram below in **Figure 3.3** shows a simple setup of XRD. XRD is again the X-rays traveling through the structures of materials and being received with a corresponding angle that can be related to crystal planes. XRD is non-destructive but produces harmful radiation and needs a thicker sample to collect sufficient data. Bragg's Law is cited below:

$$n\lambda = 2d \sin\theta \qquad (2)$$

where n is whole number, λ is wavelength, d is path difference, and θ is angle of incidence and scattering. The incident beam will hit the sample and diffract which is the goal of the detector to sense.

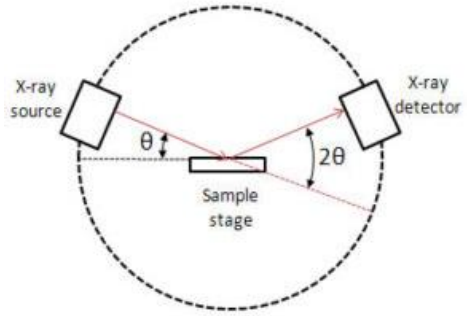

Figure 3.3 *This image is taken from X-Ray Diffractometer and Its Various Component Parts for X-Ray Studies. This illustrates Bragg's angle of the X-ray with the sample's interaction with detector and source.* [30]

One keynote when working with TMDC structures is that they have the same typical structure per family. For example, for the 2H should be the same, but will have different lattice spacing because of the different atoms being present. This can be seen in **Figure 4.5(B)** and **4.5(C)**. Though the peak intensities are different the angle of diffraction remains the same.

Again, the structure is what gives the TMDCs its properties, such as 2H-structures having superconducting capability. 1T structure is another structure which is hoped to be discovered in the data. 1T and 2H would both have different planes from one another. Also, the Cr_2S_3 also has a unique structure that would vary greatly from 1T and 2H structures. Last to see is the 1T' structure that is the intermediate of both 1T and 2H structures. Finding this structure is not needed for this experiment and is hard to find because of the randomness of the structure. For 2H, the signals are at $2\theta = 14.3^{\circ}$, 29°, 44°, and 59.7° which are correlated to the (002), (004), (006), and (008),

3.3 X-ray Photoelectron Spectroscopy

X-ray Photoelectron Spectroscopy or XPS is another method to look at the composition of the TMDCs materials. Like XRD it uses X-rays to find fingerprints of a material. XPS does use X-rays like XRD but uses X-rays to find the composition of the material rather than the structure.

3.3.1 Background

Spectroscopy is electromagnetic radiation of atoms that can be studied by wavelengths that are emitted [31]. A problem that the characterization has is that it only takes and records data from the surface of the sample. The sample is being hit by X-rays to create photoelectron emissions from the surface seen in **Figure 3.4**. Analytical which is the software and machine the sample were tested in. The machine used was also calibrated to on offset with the use of carbon. Two types of scans can be provided via this method. One is a wide scan that is an overview of

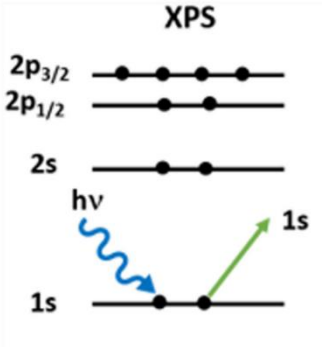

Figure 3.4 *In the image there is an incident X-ray beam hitting the samples valence shells and hitting an electron off the shell which is recorded by a detected.*

the sample composition and the other is a narrow scan that is a more detailed scan. Each element

will have a corresponding orbital that can be denoted by the binding energy that is detected from the sample. The equation that describes the photoelectric effect is:

$$E_k = hv - E_b \quad (3)$$

E_k being Kinect energy, his Planck's constant, v is frequency, and E_b is binding energy.

The samples in these samples have been sitting out and it is expected that the samples contain oxides and TMDC material. In **Figure 4.6** shows the software Kratos Analytical is used to auto detect the different peaks found in the data of characterized TMDC materials. A wide scan does not give a good enough view and narrow scans are needed to see the specific fingerprints of the electron that are being emitted.

3.4 Atomic Force Microscopy

Atomic Force Microscopy or AFM is an imaging technique to reveal the submicron surface features of a material. AFM provides 3D topographic information in addition to being nondestructive to the sample. The topographic information elucidated by this process is also simple to collect as there is a very small amount of sample prep required. In collaboration with a data visualization and analysis program called Gwyddion, the topography can be analyzed to reveal surface roughness [32].

3.4.1 Background

The functional performance of materials is critically dependent on the surface features and defects within a material. For this reason, AFM is important as it can provide high resolution images for characterization of a material. The main components of the AFM are a laser, a photodiode, a cantilever, and the tip. As the tip moves along the sample surface, the tip rises and falls based on the contact forces between the surface and tip. The laser is reflected off the cantilever and into the photodiode where the changes in laser position can be extrapolated into topographical information which is used to generate an image. The spring constant of the cantilever determines the contact forces between the tip and the surface which is easily described by Hooke's law. This equation explains the spring force as $F=kx$ where k is the spring constant of the cantilever, x is the deflection of the cantilever, and F is the force exerted onto the cantilever. An illustration of the system is shown in **Figure 3.5**.

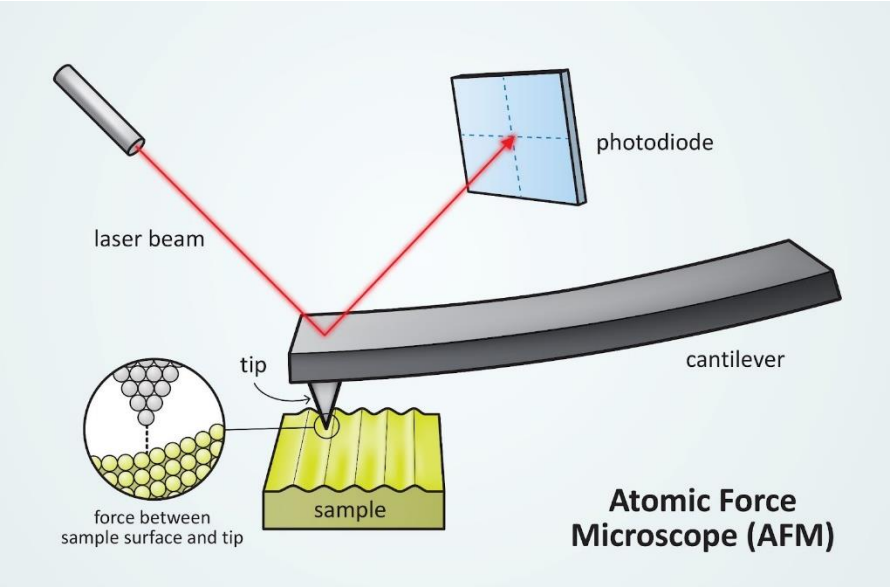

Figure 3.5 *The illustration portrays the general position of each of the main elements of the AFM, the laser, the photodiode, the cantilever, the tip, and the sample surface.* [33]

The tip sharpness will affect the clarity of results where a duller tip causes more uncertainty in measurements. With a sharper tip, less atoms on the surface will interact with the tip resulting in more atomic resolution. The AFM can perform in multiple modes; two of which are titled non-contact mode and contact mode. Each mode uses repulsive or attractive forces to operate. The contact mode measures the repulsive forces as the tip is dragged across the sample surface at a distance no less than 0.5nm. The system continuously monitors the forces and adjusts the cantilever height to maintain a constant force. The contact mode can minimally damage the surface of either the sample or the tip depending on the friction of the surface and the surface roughness. In the noncontact mode, the tip and sample never physically touch by keeping a distance of around 0.1 nm-10 nm from each other. The non-contact mode vibrates the cantilever beam at a frequency larger than its resonant frequency. Attractive van der Waals forces between

the sample and tip cause a change in vibrational frequency of the cantilever resulting in a change of the resonant frequency and a change in height of the tip, which is then recorded and transposed into an image.

4 Sample Characterization Results

4.1 Raman Spectroscopy Results and Analysis

4.1.1 Tungsten Disulfide

For the different samples the data was collected using Raman spectroscopy from the Stanford campus. The laser used in these experiments was a 532 nm laser. Data of the 3nm Tungsten sample can be seen below in **Figure 4.1**. Since this WS_2 was synthesized with metal

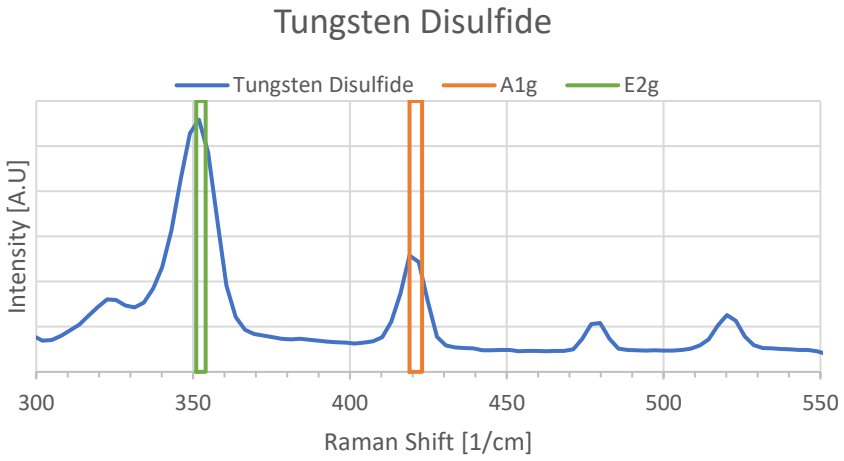

Figure 4.1 *Graphical data is the result of the Raman spectroscopy of the 3nm Tungsten Disulfide sample. The green indicates the spectrum E_{2g} can appear and A_{1g} spectrum is the orange rectangle. The peak between 450cm^{-1} and 500cm^{-1} is a sulfur peak* [42]. *The peak between 500 to 550cm^{-1} is the silicon peak.*

seeding layers it would be expected to have multiple layers. The E_{2g} peak of WS_2 is near 351 cm^{-1} and the A_{1g} is 417 cm^{-1} [34]. In **Figure 4.1** there are two distinct peaks that are present in both places. Compared to the WS_2 in figure 7 especially with the at 324 cm^{-1} which is part of WS_2 fingerprint. The other two peaks are not associated with the WS_2. The far peak at 520 nm on the

left of **Figure 4.1** is the silicon peak of the substrate. Note the silicon peak is important to properly calibrate the Raman spectroscopy spectrum.

4.1.2 Molybdenum Disulfide

Another pair of samples were two Molybdenum Disulfide samples which were fewer promising data. As seen in **Figure 4.2** there are some distinct peaks without noise, but there are no clear peaks in E_{2g} and A_{2g} positions for MoS_2 (b). Positions being approximately at E_{2g} at 382.7 cm^{-1} and A_{2g} at 407.3 cm^{-1}. For the MoS_2 (a) sample there are two small peaks, but this data doesn't contain the silicon peak which is discerning. Since this is an older sample there is

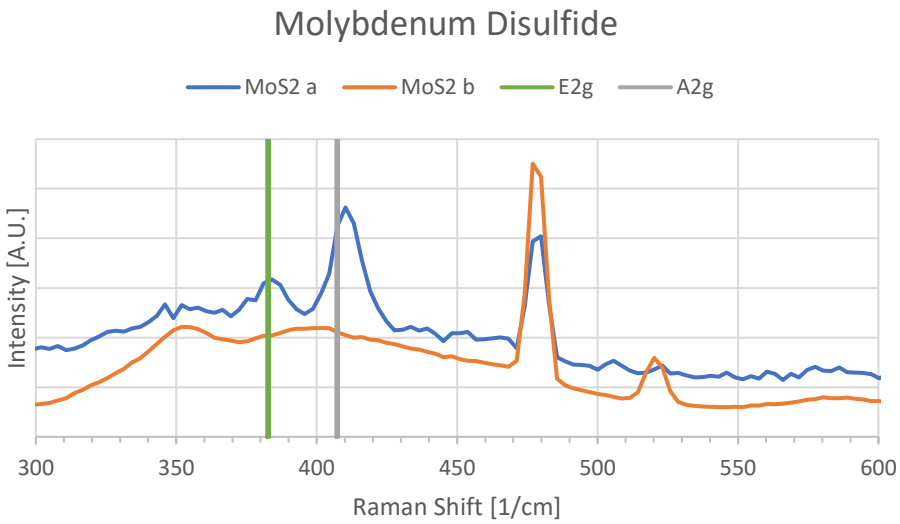

Figure 4.2 *Graph shows the Raman data of two different samples. MoS2 a is an older sample while MoS2 be is a more recently made sample. Again, the orange and green line indicate peaks from previous works [13]. The signal of Sulfur is depicted like in figure 3.3.*

possible oxidational Molybdenum film obscuring the Raman signal, or another reason is that the MoS_2 did not have the correct growth conditions within the Hong lab's CVD system. The MoS_2 (b) sample is newer and made via the same parameters.

4.1.3 Molybdenum/Chromium Disulfide

The 10 nm Molybdenum and 40 nm Chromium samples have positive results for Molybdenum Disulfide peaks and negative results for the Chromium (III) Sulfide. **Figure 4.3** is a graph of Molybdenum/Chromium sample results. Both E_{2g} and A_{1g} peaks for MoS_2 are visible for sample b. Sample A is older and has been affected by oxidation overtime. This oxidation may distort or change the composition of the TMDC sample. Like the Molybdenum Disulfide sample the older sample does not display a silicon peak which is caused by the oxidation. For the Cr_2S_3 peaks there is a 350 cm^{-1} peak for the $MoCrS_2$ b sample that is close to 344 cm^{-1} peak but there is

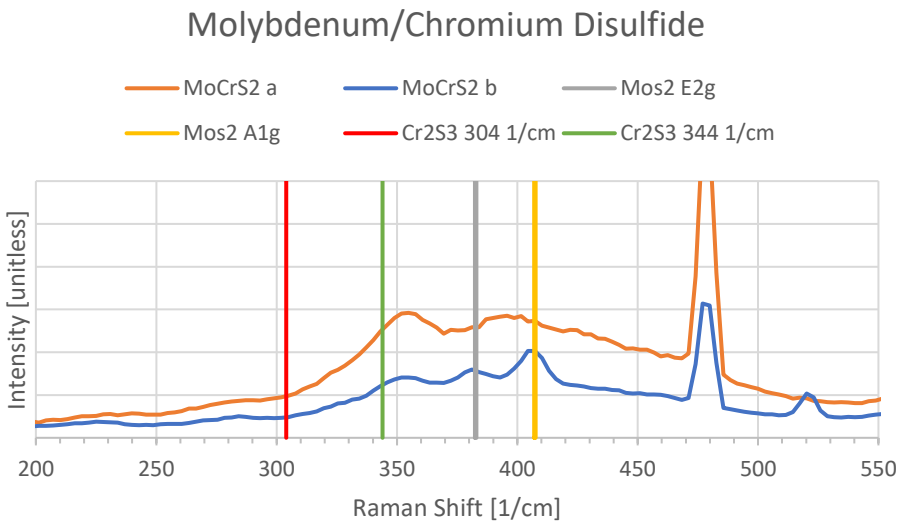

Figure 4.3 *Graph is the Raman data of the 10 nm Mo and 40 nm Cr samples made in the lab. Grey and Yellow lines are the MoS_2 Raman peaks, respectively. The green and blue lines belong to peaks associated with Cr_2S_3 peaks.*

no 304 cm^{-1} peak that is found. Possible reason is one that there was never Cr_2S_3 formed during the synthesis. The second reason the peak is not found is that the Molybdenum layer being 10 nm thick is too thick for the Raman lasers to penetrate.

4.1.4 Molybdenum/Titanium Disulfide

Lastly is the Molybdenum Titanium Disulfide sample in **Figure 4.4**. This data set has both peaks for MoS_2 for both samples $MoTiS_2$ a and $MoTiS_2$ b. For the silicon peak the older sample has a weaker peak signal than the newer sample b. For the TiS_2 there is no evidence of them since there are no E_{2g} peaks at 229.6 cm^{-1} [14]. The other peak at 382.7 cm^{-1} can be confused with MoS_2 peak. These peaks are usually paired with one another to identify the TMDCs are present, but there is only one peak and problem is either that the Raman laser is not penetrating the 10 nm thick surface of the samples or the sulfurization in the synthesis of the $MoTiS_2$ is not reaching the titanium that is coated by the Molybdenum.

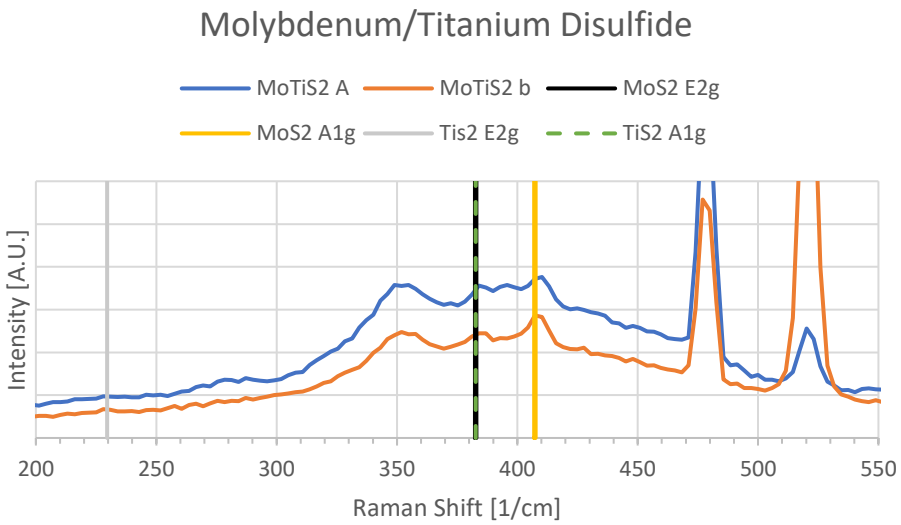

Figure 4.4 *Graph shows the Raman data set for the Molybdenum/Titanium Disulfide samples. Black and yellow lines correlate to* MoS_2*. The orange dashed and blue line are the* TiS_2 A_{1g} *and* E_{2g} *Raman peaks.*

4.1.5 Summary of Raman characterization

Creating MoS_2 and WS_2 with the metal seeding layer method is repeatable and successful. The data is clearly seen in the Raman data in all graphs. The challenge with the Raman and the synthesis is the ability to see under coated layers. Since there is no evidence of peaks Cr_2S_3, CrS_2, or TiS_2 it is fair to assume that the sulfurization process of CVD is only successfully combining with Molybdenum and not with Chromium or Titanium. Two reasons this may be happening is that the sulfur would rather bond with Mo instead of Cr or Ti because it is a more favorable reaction, or the layer of Mo is too thick for the sulfurization to penetrate to get to the titanium or chromium.

4.2 X-ray Diffraction Results and Analysis

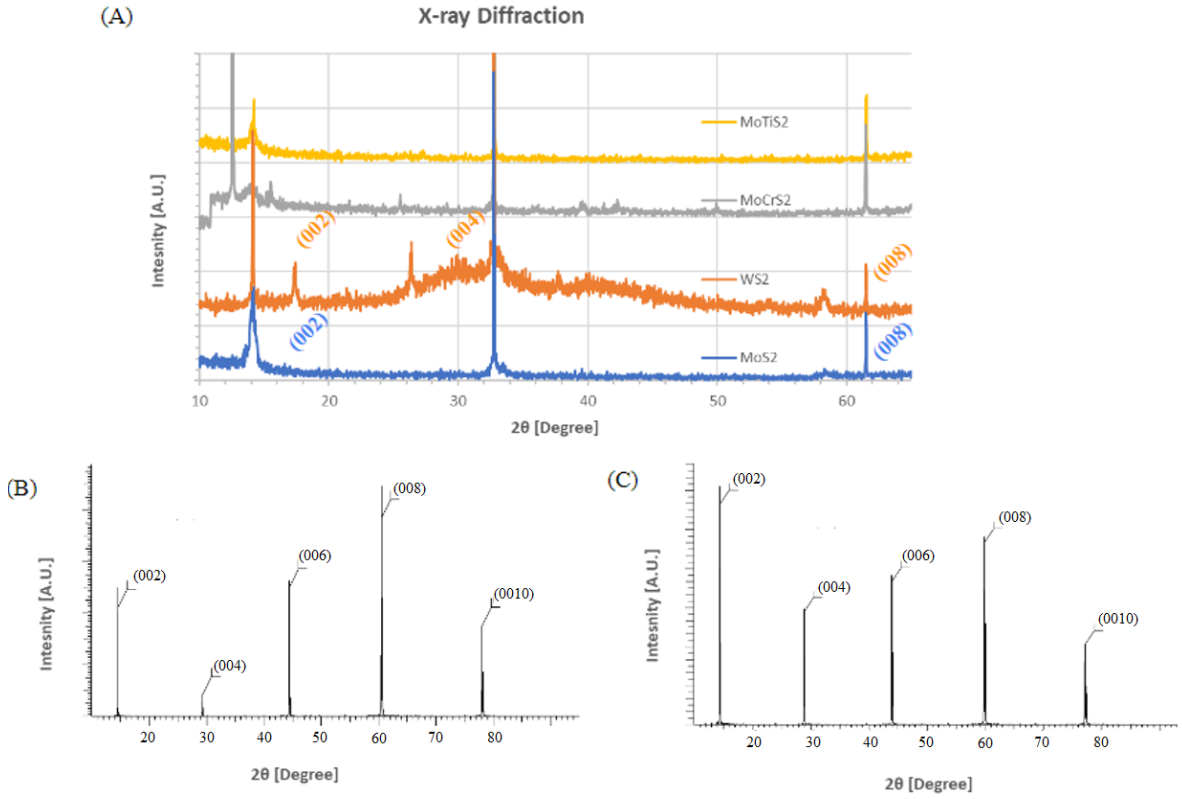

Figure 4.5 *(A) Is the experimental results of the TMDCs. (B) is the existing data on MoS_2 XRD patterns. (C) is the existing data on WS_2 XRD. (B) and (C) are previously discovered peaks* [30].

4.2.1 Tungsten Disulfide

The Tungsten Disulfide in this XRD characterization was the older sample that was made around 40 nm thick, but for the data in **Figure 4.5A** has similar peaks compared to other samples at $2\theta = 14.3^{\circ}$, 29°, and 59.7° related to the planes (002), (004), and (008), respectively. There are

Figure 4.6 *(A) Is the experimental results of the TMDCs. (B) is the existing data on MoS_2 XRD patterns. (C) is the existing data on WS_2 XRD. (B) and (C) are previously discovered peaks* [35].

more planes that can be found by XRD, but these planes are the ones with noticeable peaks in the data. The peaks can show that Tungsten Disulfide has been created and present in the sample, but with the sample it has degraded overtime in the open air by oxygen. The oxidation of the sample can explain the extra existing peaks within the data. Other reasons that there are extra XRD peaks reading is that these peaks are artifacts that don't exist, or the sample has been contaminated because all the movement and travel the sample has been through. There is an unknown peak at 32.1°, this is probably from the oxides forming or most likely the Silicon substrate of the sample.

4.2.2 Molybdenum Disulfide

It is known that Molybdenum disulfide peaks found at $2\theta = 14.3^{\circ}$, 29°, 44°, and 59.7° which are correlated to the (002), (004), (006), and (008), respectively [35]. The problem with sample in **Figure 4.5** below is that the data does not display all peaks/planes that have been found in previous data. The (002) and (008), are clear in **Figure 4.5**, but all other peaks are not there or barely present. With this information the MoS_2 is not present at all or with the Raman data, the data can confirm that the MoS_2 is there in the sample. There are only a few peaks which could mean the sulfurization process is not sufficient and there are no peaks to be observed or that XRD could not pick up the peaks. Beside these peaks there are no real comparisons in previous data of MoS_2 and Molybdenum Oxide that can be made making it seem like MoS_2 was not successfully made. Displays the at $2\theta = 32.1^{o}$ peak like the Molybdenum with the same reasoning.

4.2.3 **Molybdenum/Chromium Disulfide**

The prime sample that was looked at was the double layer metal seeding layers. In **Figure 4.5(A)** this is the XRD data, received from the campus's XRD, that contain both double transition metal layers that were sulfurized There are no other distinguishable fingerprints that can be matched to this data especially for the Cr_2S_3 peaks [36]and the silicon peaks in **Figure 4.5(A)**. This can affirm that the sulfurization cannot penetrate the Molybdenum layer and combine with the chromium layers below. Otherwise, that would mean that XRD cannot detect anything past the Molybdenum layers since there is no detection of silicon or a Cr_2S_3 structure. Again the (002) and (008) are present meaning that there is a TMDC.

4.2.4 Molybdenum/Titanium Disulfide

In comparison to the other sample with double transition metal layers this did not get as promising results with the Molybdenum Disulfide seen in **Fig. 4.5**. For the peaks at $2\theta = 14.3^{\circ}$ and 59.7° are only obvious peaks in the graph. There are no other peaks that match existing TiS_2 XRD peaks data[37], only exhibiting the MoS_2. This makes it more obvious that the XRD laser is penetrating the sample and is detecting the silicon underneath the two TMDCs layers. So, the Cr_2S_3 or the TiS_2 are not successfully created in the seeding layer because the Molybdenum coated is either too thick for sulfur to penetrate through, the Molybdenum sulfurization is preferable, or the Molybdenum a great seal that stop the sulfurization all together. For just **4.5(A)** there are many materials involved that may stop the ability to get a clear image or it can be the fault of the machine. Two peaks for MoS_2 are evidence, but having all peaks is preferred to get a

better confirmation. Otherwise using XRD in tandem with Raman shows promising results that there is 2H-TMDC present.

4.2.5 Summary of XRD experiments

XRD in this experiment has shown that the layers exposed to the surface in each sample are the ones to more successfully sulfurize while the other layers seem to be untouched. These exposed layers have one or two peaks of planes that resemble the structures that the different TMDCs have. In some instances, the signals were too weak to be detected, which could be attributed to improper sulfurization, malfunctioning equipment, or the formation of an obstructive layer on the TMDC material. However, when considering the Raman spectroscopy data, it's evident that Molybdenum and Tungsten Disulfide can be consistently synthesized using the metal seeding layer technique. One last note on the XRD data is that there are similar peaks at $2\theta = 14.3^{\circ}$, 29°, and 59.7°. TMDCs should have similar structures because they all have the same structure of 2H. Comparing both Molybdenum Disulfide and Molybdenum/Titanium Disulfide, they have similar peaks that match and are indistinguishable from one another which can make it hard to know if there are different TMDCs, especially for the double layered TMDCs. The only way to distinguish between the TMDCs is different structures.

4.3 X-ray Photoelectron Spectroscopy Results and Analysis

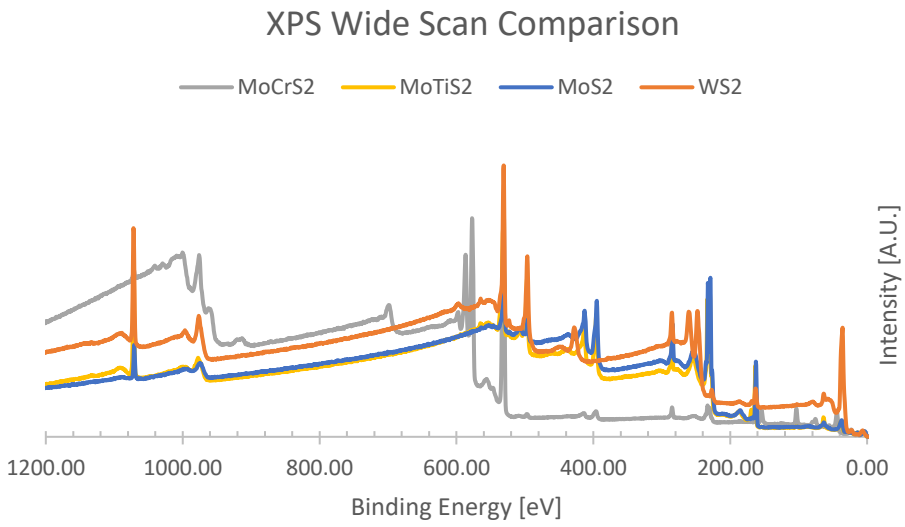

Figure 4.7 *XPS wide spectra for the TMDC layers both double layer and single.*

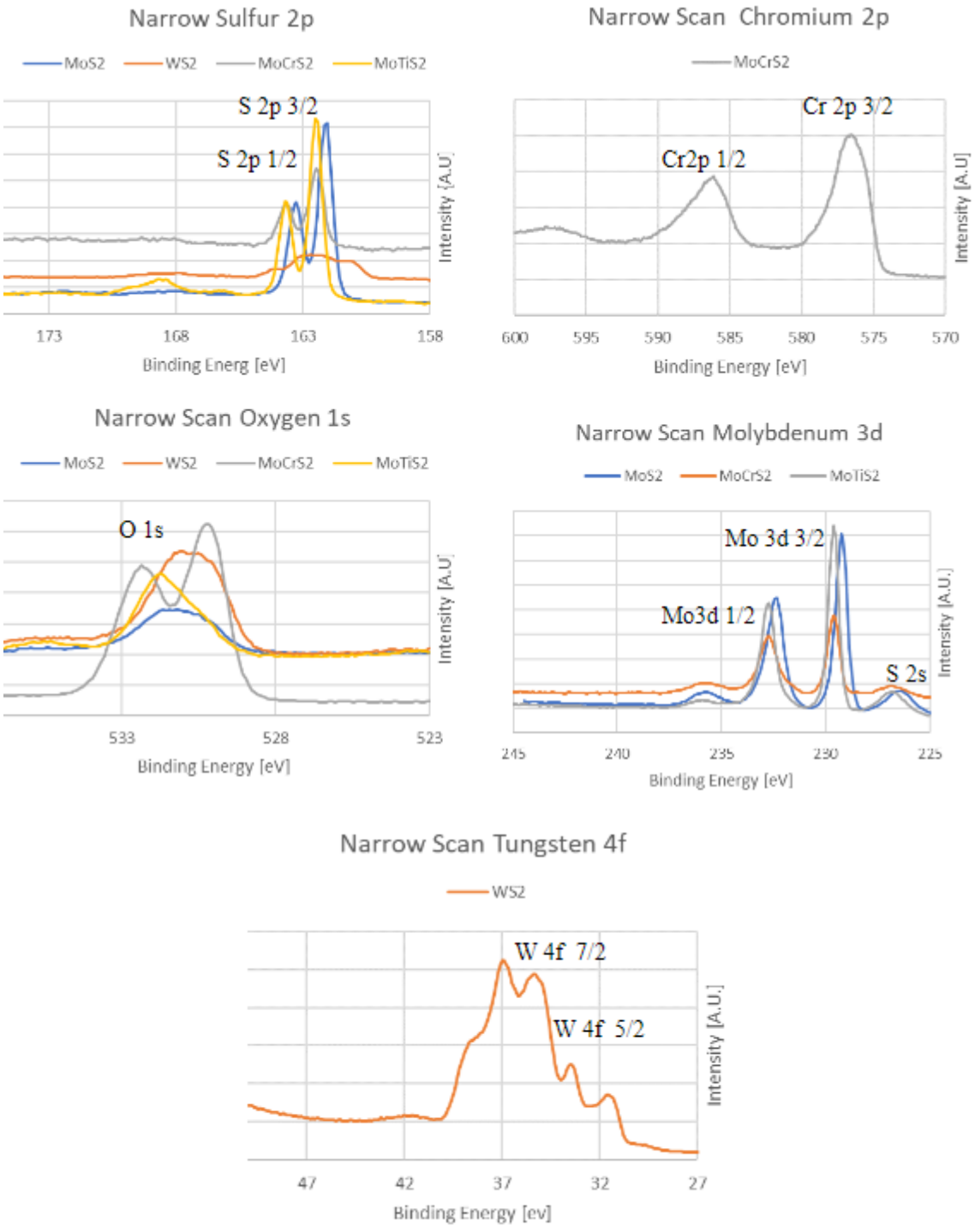

Figure 4.8 *The figures show all narrow XPS that had detectable peaks with Kratos Analytical.*

4.3.1 Tungsten Disulfide

In this research all samples were subjected to XPS. One to note is the WS_2 samples which are seen in **Fig. 4.7** have similar peaks to existing data and Kratos Analytical [38], [39]. The 7/2 and 5/2 peaks are there in the XPS data for **Fig. 4.7**, but there seems to be extra appearing peaks which may be an occurrence of oxidation occurring on the sample or artifacts being created by the characterization. system. **Figure 4.7** shows the Sulfur peaks which have a rough outline image but shows similar traits to existing sulfur peaks [38], [39]. **Figure 4.7** illustrates the narrow scan for the oxygen peaks that occur on the sample. The importance of all these narrow scans with XPS is to detect composition of the materials. As seen in **Figure 4.7** there are signals in all narrow scans of the samples. Having both Tungsten and Sulfur can confirm that there is WS_2 in the sample, but with the presence of oxygen in the XPS data that also means that there are Tungsten Oxides. With data this means that the surface of this sample is a mixture of both Tungsten Oxides and WS_2.

4.3.2 Molybdenum Disulfide

The Molybdenum samples in **Figure 4.7** have the definite shape and ranges for the MoS_2 composition. The data for Molybdenum does have the 3 peaks two being Mo peaks: 3d 5/2 and 3/2 peaks while the other being the 2s Sulfur peak. There is one more extra peak around the 236-eV range. When using the software to identify the binding energies to composition there is no element that matches with this specific range. This peak might be an artifact or noise created by the characterization or it is contamination of the sample from another source. The data found on the Sulfur peaks resemble previous works with the 2p 1/2 and 3/2 peaks [38], [40]. Again, the oxygen peak of the MoS_2 sample fits the fingerprint, but the only note is that the data is wider or

has more sub peaks than existing data[40]. From this data there is MoS_2 by the evident Mo and S peaks in the corresponding binding energies. Molybdenum Oxide can be occurring in this sample, but the range discrepancy is a bit odd. Generally, TMDC materials will oxidize because of the nature of stability.

4.3.3 Molybdenum/Chromium Disulfide

The double transition metal layered XPS data is displayed in **Figure 4.7**. Compared to previous data Chromium has the two distinct peaks at 3/2 and 1/2 which this data has, **Figure 4.7 A**. The only problem is that Chromium should not be visible in the data because it is covered by 10 nm of Molybdenum that should not allow XPS scans to reach it. The reason that the Chromium is popping up in scan is that there might be a scratch that reaches down to the Chromium. The data should look to have no peaks where the data is indiscernible. Otherwise, this does confirm that Chromium is present in the material. XPS data for the Molybdenum looks like the Molybdenum Chromium samples. Both have the same characteristic double Molybdenum peaks with both the extra unknown peak and the sulfur 2s peak. The Oxide scan was different because the oxide peak is split into two peaks. There might be some Oxides forming with the metals with this data. It is easier to affirm that Molybdenum Disulfide is present since it is on the surface of the sample than Chromium Disulfide which should cover Molybdenum. It could be possible that Cr and S are forming with each other, but all other sources don't point towards that direction. MoS_2 fingerprint checks out with existing data, but CrS_2/Cr_2S_3 does not check out.

4.3.4 Molybdenum/Titanium Disulfide

The next sample is another double layered TMDC that contains Titanium instead of Chromium referenceable in **Figure 4.7**. The Molybdenum should stop any source of XPS from reaching the Titanium which would appear with no peaks in a XPS graph. Compared to other XPS, there are no strong signal occurring that can be found which is evidence that the Molybdenum has stopped the Titanium from sulfurizing. The only flaw in this is that the temperature to sulfurize Titanium was not high enough. On the other hand, the Molybdenum placed on the surface of the sample got to interact with the Sulfur resulting in more similar data than all other Molybdenum displayed with similar binding energies rather than intensity. Data can conclude with the two sulfur peaks that resemble MoS_2 peaks at S 2p 1/2 and 2p 3/2. There is another peak in Sulfur scan that is before double Sulfur peaks, but that peak does not have any relation to any orbital via the software of Kratos Analytical. The Oxygen peaks look most like existing XPS data and have more of a point for the peaks than in the other figures and datasets. This results in Molybdenum Oxide residing on the surface of the sample in addition to the MoS_2.

4.3.5 Summary of XPS characterizations

All XPS data gives sufficient XPS information to claim that there are TMDCs on the surfaces of each individual material tested. All datasets have the same distinct Sulfur 2p peaks in 160-165 eV range. The materials that have outer layers coated in Molybdenum have the associated Molybdenum 3d and Sulfur 2s peaks for MoS_2. The Tungsten Disulfide samples did have the associated peaks but had alternate peaks that can disrupt confirmation of the composition. With the help of the other characterization, it can be confirmed that MoS_2 and WS_2 are successfully made.

4.4 Atomic Force Microscopy Result and Analysis

4.4.1 Tungsten Disulfide

After investigating all the samples with AFM, it was determined that Tungsten disulfide (WS_2) sample B had the most promising discoveries. WS_2 sample B was covered in approximately 60% WS_2 based on optical images. The makeup of approximately 40% of the sample was either larger nucleation sites or a purple color which is the silicon substrate underneath that the WS_2 was epitaxially grown on. **Figure 4.8** shows an image of the sample with an optical microscope image next to it, further illustrating the light blue and purple locations on the sample.

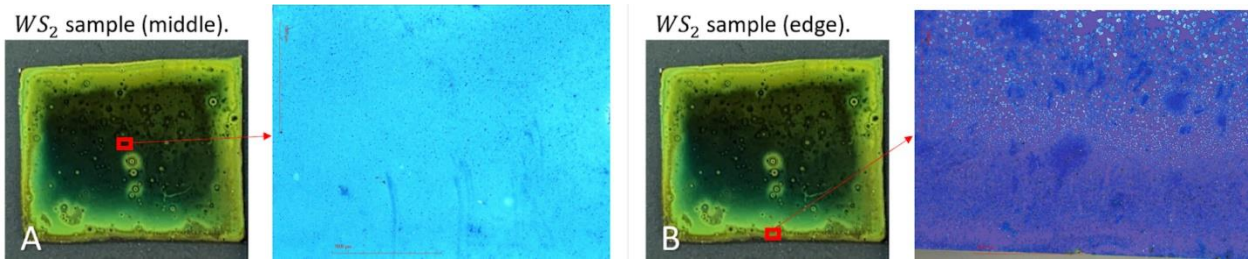

Figure 4.9 *A) shows an image of the WS_2 sample with a cutout of the optical image at the middle of the sample. B) shows an image of the WS_2 sample with a cutout of the optical image at the bottom edge of the sample.*

To perform the AFM, a TESP tip made by Veeco was used in the non-contact mode. Due to a limited selection of tips and the limited reliability of results using other tips, the TESP tip was chosen. It provided the highest resolution images with an easy alignment process during setup. The TESP tip was designed for non-contact mode so by default, that mode was chosen. The added benefit of studying the thin 3nm thick tungsten on the silicon sample with the non-

contact mode is that the non- contact mode is nondestructive. The tip is etched in silicon and has a radius of 7nm.

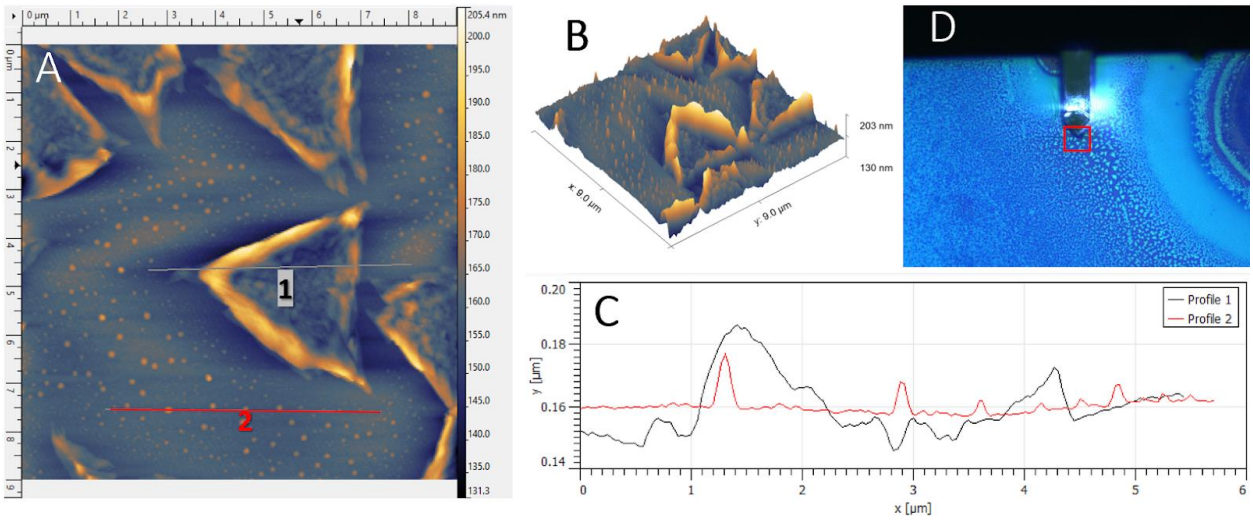

Figure 4.10 *A) shows an AFM image of the WS_2 sample completed in the program Gwyddion. B) shows a 3D image of the same location. C) shows a height profile of the two lines on image A, the red line corresponds to the 2nd line and shows it is relatively flat compared to the gray line atop the triangular structure. D) shows the optical microscope image of the location of the AFM squared in red.*

Figure 4.9 shows an AFM scan on one section of the WS_2 sample B. Many distinct light blue triangles can be seen in the optical image figure 3.14(D). Using the AFM, the 3D view (B) and the 2D view (A) can be analyzed. The gray and red lines on the 2D image correspond to the gray and red lines on the graph in figure 3.14(C). The y axis shows the height difference as the line progresses from left to right. The gray line shows how the height changes over the triangle structures. The triangles appear hollow with the walls protruding as much as 30nm higher than the average level surrounding them as depicted by the red line in the graph (C). The average roughness of the sample at the location in Figure 3.14 is 4.625nm. The length of the sides of the

triangle in **Figure 4.9(A)** is 3.52nm. The difference in height around the edges of the triangles could be attributed to oxidized WS_2 monolayers[46] causing an increased height. AFM was performed exactly 1 month after the WS_2 samples were created and stored in the atmosphere. The XPS results confirm these AFM findings by showing a large oxygen peak in the WS_2 sample.

The light blue colors and triangle structures shown in **Figure 4.9(D)** appear in approximately 60% of the sample surface. The size and orientation of triangles are not uniform but envelop the surface with the larger triangles concentrated near nucleation sites. A more uniform light blue is seen towards the middle of the sample, away from any nucleation sites like is shown in **Figure 4.9(A).**

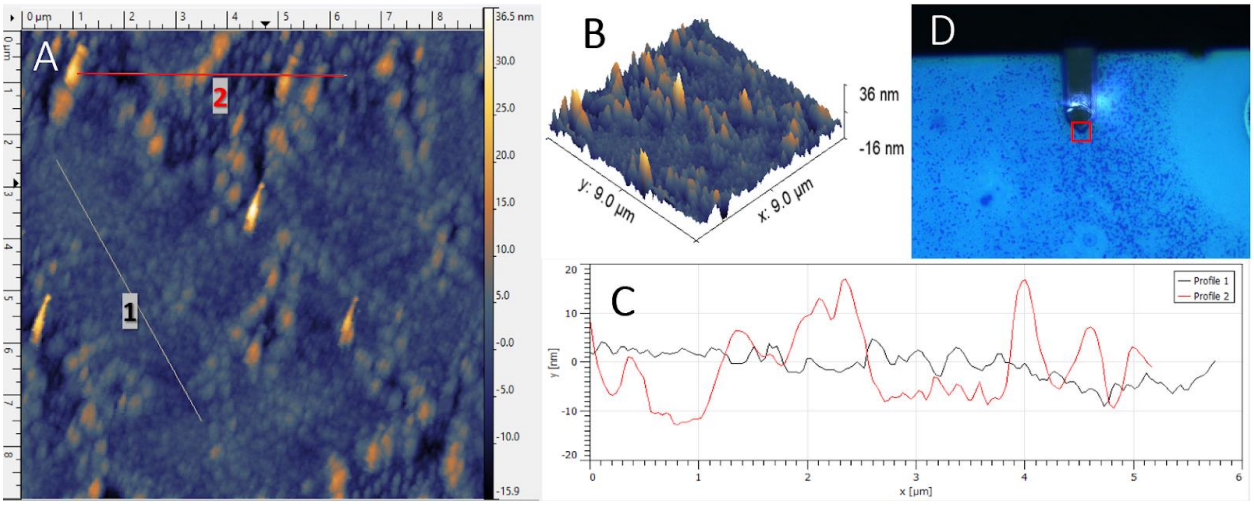

Figure 4.11 *(A) shows a 9µm x 9µm AFM image of the WS_2 sample compiled in the program Gwyddion. (B) shows a 3D image of the same location. (C) shows a height profile of the two*

Figure 4.10 shows a more uniformly light blue region with an average surface roughness of 3.110nm. **Figure 4.10(A)** shows the 2D AFM image and two lines, one gray and one red. The gray line lies within the interior of the light blue material. It is rough on the inside and has "walls" with a larger height which is indicated by a more orange coloration in **Figure 4.10(A)**.

The darker blue color within **Figure 4.10 (A)** has a lower height and is shown clearly by the red line labeled “2”. **Figure 4.10 (C)** shows the height profile of the two lines. The dark blue regions in **Figure 4.10 (A)** correlate to the purple regions in the optical image, **Figure 4.10(D)**. **Figure 4.10(B)** shows a 3D rendering where the differences in height along the AFM image are clear. The difference in height between the dark blue and orange areas in **Figure 4.10(A)** is around 30 nm which is the same as the AFM shown in **Figure 4.9**. This indicates that the height difference in these two different regions is the same, indicating an even distribution of WS_s atop the silicon substrate. Both AFM images in **Figures 4.9** and **4.10** were taken near the center of WS_2 sample B.

4.4.2 Summary of AFM characterizations

The optical images show the WS2 sample B has some uniformity near to the middle of the sample only broken up by defects like nucleation sites. Both AFM images show hollow formations with tall walls. More distinct and larger triangles surround the nucleation sites. The walls are hypothesized to be oxidation sites due to the large amount of oxygen in the Raman data and the 1 month waiting period between making the sample to performing AFM on it. Due to these triangles, the surface roughness reached 4.625nm around the AFM location in **Figure 4.9(A)**. However, the locations with more uniformity in the light blue color show an average roughness of 3.110nm. Because WS_2 oxidizes into WO_2 or WO_3, the total amount of WS_2 diminishes over time leading to potentially reduced performance. In conjunction with Raman Spectroscopy, the AFM could be used in further testing to apply voltage and force oxidation on the sample to help elucidate the composition of the raised surfaces on the sample which as of now are believed to be oxidized tungsten[41]. Further monitoring of the oxidation state of the

sample could help in determining a lifetime for the sample. More AFM experiments will be conducted to provide insight into the uniformity of the other WS_2 samples grown at different temperatures and pressures with the goal of creating the most uniformity possible.

5 Conclusion

The TMDCs that are made with metal seeding layer method have promising results. Though there are problems that arise with oxidation occurring in the surface of the samples, there are many things to note with all the following different characterizations.

1) The results of the seeding layer method show that the outer surfaces like Tungsten Disulfide and Molybdenum Disulfide are present with their two fingerprint peaks. In XPS, all samples have the necessary peaks for either Tungsten Disulfide or Molybdenum Disulfide. The flaw in XPS is that it can only sample the surface and not penetrate lower layers like Titanium or Chromium. Using XPS would be better used after synthesizing of a single transition metal layer of CVD. The composition methods show that MoS_2 and WS_2 have prominent peaks in the data.
2) TMDCs tend to have similar structures and the incident angles are found to be similar with each test and previous results. The problem is that the structures of the TMDCs can be confused from one another when it comes to double layers of transition metals.
3) Atomic Force Microscopy can look at surface structure, but at a broader level than atomic. The Tungsten Disulfide had triangular shapes that mirror data from previous studies[41]. The structure found was triangle growth that were surrounded by wall of oxidation.

Employing a full spectrum of characterization methods is crucial for validating the composition and structure of TMDCs. The prevalent challenge across all TMDCs is the tendency for surface oxidation, which can significantly degrade the yield and quality of their unique properties. Samples with Titanium and Chromium in the TMDC composition were samples that

had high oxidation rate while Molybdenum and Tungsten in the TMDC composition. Molybdenum was utilized as a protective layer to inhibit the oxidation of Titanium, but its high efficiency also prevents the sulfurization of both Titanium and Chromium. The characterization methods used were unable to distinguish between the structures of Titanium and Molybdenum, making it difficult to differentiate between the two in terms of their structural aspects.

There's a multitude of potential avenues for exploration. One possibility is to experiment with the thickness of the Molybdenum layer, seeking a balance that permits sulfurization while also mitigating oxidation in compounds such as Titanium Disulfide or mixtures involving Chromium and Sulfur. An alternative tactic is to omit Molybdenum layers altogether, promptly analyzing samples like TiS2 before any chance of oxidation. Methods like applying a sealing coat to TiS_2, $Cr2S_3$, and CrS_2, or cryogenically freezing the samples, could also serve to protect against oxidation. The scope of testing should not be limited to Ti and Cr; W, Mo, and even the application of metal seeding layers to other transition metals like Nickel, Niobium, or Vanadium is viable. Additionally, performing new AFM evaluations on Cr and Ti samples could shed light on the structural evolutions and the tempo of TMD oxidation.

References

[1] Q. H. Wang, K. Kalantar-Zadeh, A. Kis, J. N. Coleman, and M. S. Strano, "Electronics and optoelectronics of two-dimensional transition metal dichalcogenides," *Nat Nanotechnol*, vol. 7, no. 11, pp. 699–712, 2012, doi: 10.1038/nnano.2012.193.

[2] K. Chen *et al.*, "Diverse electronic and magnetic properties of CrS2 enabling strain-controlled 2D lateral heterostructure spintronic devices," *NPJ Comput Mater*, vol. 7, no. 1, p. 79, 2021, doi: 10.1038/s41524-021-00547-z.

[3] G. Y. Guo and W. Y. Liang, "The electronic structures of platinum dichalcogenides: PtS2, PtSe2 and PtTe2," *Journal of Physics C: Solid State Physics*, vol. 19, no. 7, p. 995, 1986, doi: 10.1088/0022-3719/19/7/011.

[4] A. H. Reshak and S. Auluck, "Electronic and optical properties of the 1T phases of TiS2, TiSe2, and TiTe2," *Phys Rev B*, vol. 68, no. 24, p. 245113, 2003, doi: 10.1103/PhysRevB.68.245113.

[5] A. Aljarb *et al.*, "Substrate Lattice-Guided Seed Formation Controls the Orientation of 2D Transition-Metal Dichalcogenides," *ACS Nano*, vol. 11, no. 9, pp. 9215–9222, 2017, doi: 10.1021/acsnano.7b04323.

[6] Y. Zhan, Z. Liu, S. Najmaei, P. M. Ajayan, and J. Lou, "Large-Area Vapor-Phase Growth and Characterization of MoS2 Atomic Layers on a SiO2 Substrate," *Small*, vol. 8, no. 7, pp. 966–971, 2012, doi: https://doi.org/10.1002/smll.201102654.

[7] Y. Shi *et al.*, "van der Waals Epitaxy of MoS2 Layers Using Graphene As Growth Templates," *Nano Lett*, vol. 12, no. 6, pp. 2784–2791, 2012, doi: 10.1021/nl204562j.

[8] S. Manzeli, D. Ovchinnikov, D. Pasquier, O. V Yazyev, and A. Kis, "2D transition metal dichalcogenides," *Nat Rev Mater*, vol. 2, no. 8, p. 17033, 2017, doi: 10.1038/natrevmats.2017.33.

[9] J. Chu *et al.*, "Sub-millimeter-Scale Growth of One-Unit-Cell-Thick Ferrimagnetic Cr2S3 Nanosheets," *Nano Lett*, vol. 19, no. 3, pp. 2154–2161, 2019, doi: 10.1021/acs.nanolett.9b00386.

[10] F. Kafi, R. Pilevar Shahri, M. R. Benam, and A. Akhtar, "Tuning Optical Properties of MoS 2 Bulk and Monolayer Under Compressive and Tensile Strain: A First Principles Study," *J Electron Mater*, vol. 46, pp. 6158–6166, 2017.

[11] K. F. Mak, C. Lee, J. Hone, J. Shan, and T. F. Heinz, "Atomically Thin MoS2: A New Direct-Gap Semiconductor," *Phys Rev Lett*, vol. 105, no. 13, p. 136805, 2010, doi: 10.1103/PhysRevLett.105.136805.

[12] J. Gusakova *et al.*, "Electronic Properties of Bulk and Monolayer TMDs: Theoretical Study Within DFT Framework (GVJ-2e Method)," *physica status solidi (a)*, vol. 214, no. 12, p. 1700218, 2017, doi: https://doi.org/10.1002/pssa.201700218.

[13] M. Bolhuis, J. Hernandez-Rueda, S. E. van Heijst, M. Tinoco Rivas, L. Kuipers, and S. Conesa-Boj, “Vertically-oriented MoS2 nanosheets for nonlinear optical devices,” *Nanoscale*, vol. 12, no. 19, pp. 10491–10497, 2020, doi: 10.1039/D0NR00755B.

[14] M. A. Bissett, S. D. Worrall, I. A. Kinloch, and R. A. W. Dryfe, “Comparison of Two-Dimensional Transition Metal Dichalcogenides for Electrochemical Supercapacitors,” *Electrochim Acta*, vol. 201, pp. 30–37, 2016, doi: https://doi.org/10.1016/j.electacta.2016.03.190.

[15] W. Choi, N. Choudhary, G. H. Han, J. Park, D. Akinwande, and Y. H. Lee, “Recent development of two-dimensional transition metal dichalcogenides and their applications,” *Materials Today*, vol. 20, no. 3, pp. 116–130, 2017, doi: https://doi.org/10.1016/j.mattod.2016.10.002.

[16] H. Li *et al.*, “Fabrication of Single- and Multilayer MoS2 Film-Based Field-Effect Transistors for Sensing NO at Room Temperature,” *Small*, vol. 8, no. 1, pp. 63–67, 2012, doi: https://doi.org/10.1002/smll.201101016.

[17] Z. Thiehmed, A. Shakoor, and T. Altahtamouni, “Recent advances in WS2 and its based heterostructures for water-splitting applications,” *Catalysts*, vol. 11, no. 11, p. 1283, 2021.

[18] X. Liu *et al.*, “A MoS2/Carbon hybrid anode for high-performance Li-ion batteries at low temperature,” *Nano Energy*, vol. 70, p. 104550, 2020.

[19] Y. Jung, J. Shen, Y. Liu, J. M. Woods, Y. Sun, and J. J. Cha, “Metal Seed Layer Thickness-Induced Transition From Vertical to Horizontal Growth of MoS2 and WS2,” *Nano Lett*, vol. 14, no. 12, pp. 6842–6849, 2014, doi: 10.1021/nl502570f.

[20] D. Kong *et al.*, “Synthesis of MoS2 and MoSe2 Films with Vertically Aligned Layers,” *Nano Lett*, vol. 13, no. 3, pp. 1341–1347, 2013, doi: 10.1021/nl400258t.

[21] D. S. Gavhane, A. D. Sontakke, and M. A. van Huis, “Selective Vertical and Horizontal Growth of 2D WS2 Revealed by In Situ Thermolysis using Transmission Electron Microscopy,” *Adv Funct Mater*, vol. 32, no. 1, p. 2106450, Jan. 2022, doi: https://doi.org/10.1002/adfm.202106450.

[22] F. Zhang *et al.*, “Controlled synthesis of 2D transition metal dichalcogenides: from vertical to planar MoS2,” *2d Mater*, vol. 4, no. 2, p. 25029, 2017, doi: 10.1088/2053-1583/aa5b01.

[23] S. Swann, “Magnetron sputtering,” *Physics in Technology*, vol. 19, no. 2, p. 67, 1988, doi: 10.1088/0305-4624/19/2/304.

[24] J. T. Gudmundsson and D. Lundin, “1 - Introduction to magnetron sputtering,” in *High Power Impulse Magnetron Sputtering*, D. Lundin, T. Minea, and J. T. Gudmundsson, Eds., Elsevier, 2020, pp. 1–48. doi: https://doi.org/10.1016/B978-0-12-812454-3.00006-1.

[25] E. Smith and G. Dent, *Modern Raman spectroscopy: a practical approach*. John Wiley & Sons, 2019.

[26] J. R. Ferraro, *Introductory raman spectroscopy*. Elsevier, 2003.

[27] M. A. Pimenta, E. del Corro, B. R. Carvalho, C. Fantini, and L. M. Malard, “Comparative Study of Raman Spectroscopy in Graphene and MoS2-type Transition Metal Dichalcogenides,” *Acc Chem Res*, vol. 48, no. 1, pp. 41–47, 2015, doi: 10.1021/ar500280m.

[28] K. Gołasa *et al.*, “Resonant Raman scattering in MoS2—From bulk to monolayer,” *Solid State Commun*, vol. 197, pp. 53–56, 2014, doi: https://doi.org/10.1016/j.ssc.2014.08.009.

[29] A. Chauhan and P. Chauhan, “Powder XRD technique and its applications in science and technology,” *J Anal Bioanal Tech*, vol. 5, no. 5, pp. 1–5, 2014.

[30] “X-Ray Diffractometer and Its Various Component Parts for X-Ray Studies.,” *XRD.co*. 2017.

[31] J. M. Hollas, *Modern spectroscopy*. John Wiley & Sons, 2004.

[32] M. K. Khan, Q. Y. Wang, and M. E. Fitzpatrick, “1 - Atomic force microscopy (AFM) for materials characterization,” in *Materials Characterization Using Nondestructive Evaluation (NDE) Methods*, G. Hübschen, I. Altpeter, R. Tschuncky, and H.-G. Herrmann, Eds., Woodhead Publishing, 2016, pp. 1–16. doi: https://doi.org/10.1016/B978-0-08-100040-3.00001-8.

[33] E. Maletz, “Atomic Force Microscope Illustration.” 2016. Accessed: Aug. 27, 2023. [Online]. Available: https://www.google.com/url?sa=t&rct=j&q=&esrc=s&source=web&cd=&cad=rja&uact=8&ved=2ahUKEwiQlMPSh5qCAxXikWoFHSw2BasQFnoECA8QAQ&url=https%3A%2F%2Fprism.ucalgary.ca%2Fbitstreams%2Ffee4f7df-3cba-414b-a68c-7cc1061beefd%2Fdownload&usg=AOvVaw3MiA_0LgEP3omp-dTGKTq0&opi=89978449

[34] A. Berkdemir *et al.*, “Identification of individual and few layers of WS2 using Raman Spectroscopy,” *Sci Rep*, vol. 3, no. 1, p. 1755, 2013, doi: 10.1038/srep01755.

[35] HQ Graphene, “High quality 2D Crystals,.” Accessed: Oct. 27, 2023. [Online]. Available: https://www.hqgraphene.com\

[36] T. A. Shifa, R. Mazzaro, V. Morandi, and A. Vomiero, “Controllable synthesis of 2D nonlayered Cr2S3 Nanosheets and their Electrocatalytic activity toward oxygen evolution reaction,” *Frontiers in Chemical Engineering*, vol. 3, p. 703812, 2021.

[37] M. Parvaz, S. Ahmed, M. B. Khan, Rahul, S. Ahmad, and Z. H. Khan, “Synthesis of TiS2 nanodiscs for supercapacitor application,” *AIP Conf Proc*, vol. 1953, no. 1, p. 30121, 2018, doi: 10.1063/1.5032456.

[38] A. P. Shpak, A. M. Korduban, L. M. Kulikov, T. V Kryshchuk, N. B. Konig, and V. O. Kandyba, “XPS studies of the surface of nanocrystalline tungsten disulfide,” *J Electron Spectros Relat Phenomena*, vol. 181, no. 2, pp. 234–238, 2010, doi: https://doi.org/10.1016/j.elspec.2010.05.030.

[39] D. Barreca, G. Carta, A. Gasparotto, G. Rossetto, E. Tondello, and P. Zanella, “A Study of Nanophase Tungsten Oxides Thin Films by XPS,” *Surface Science Spectra*, vol. 8, no. 4, pp. 258–267, 2003, doi: 10.1116/11.20020801.

[40] N. P. Kondekar, M. G. Boebinger, E. V Woods, and M. T. McDowell, “In Situ XPS Investigation of Transformations at Crystallographically Oriented MoS2 Interfaces,” *ACS Appl Mater Interfaces*, vol. 9, no. 37, pp. 32394–32404, 2017, doi: 10.1021/acsami.7b10230.

[41] K. Kang *et al.*, “Graphene-Assisted Antioxidation of Tungsten Disulfide Monolayers: Substrate and Electric-Field Effect,” *Advanced Materials*, vol. 29, no. 18, p. 1603898, 2017, doi: https://doi.org/10.1002/adma.201603898.

[42] C. Nims, B. Cron, M. Wetherington, J. Macalady, and J. Cosmidis, “Low frequency Raman Spectroscopy for micron-scale and in vivo characterization of elemental sulfur in microbial samples,” *Sci Rep*, vol. 9, no. 1, p. 7971, 2019, doi: 10.1038/s41598-019-44353-6.